Copy No. 1

RM No. A7F30

RESEARCH MEMORANDUM

A SUGGESTED METHOD OF ANALYZING FOR TRANSONIC FLUTTER OF CONTROL SURFACES BASED ON AVAILABLE EXPERIMENTAL EVIDENCE

By

Albert L. Erickson and Jack D. Stephenson

Ames Aeronautical Laboratory
Moffett Field, Calif.

NATIONAL ADVISORY COMMITTEE
FOR AERONAUTICS
WASHINGTON
December 16, 1947

NACA RM No. A7F30

NATIONAL ADVISORY COMMITTEE FOR AERONAUTICS

RESEARCH MEMORANDUM

A SUGGESTED METHOD OF ANALYZING FOR TRANSONIC FLUTTER OF CONTROL SURFACES BASED ON AVAILABLE EXPERIMENTAL EVIDENCE

By Albert L. Erickson and Jack D. Stephenson

SUMMARY

This report presents the results of a study of the movement of shocks on a three-dimensional wing with and without aileron flutter occurring. The studies include a number of changes and variations to the wing and control. From these data and some basic considerations of the cause and mechanism of what may be termed "transonic flutter," a tentative method of analysis is developed. The results of the tests are presented, followed by a general discussion and specific design recommendations. It is shown that the transonic flutter is caused by a lag in build-up of the resultant hinge moment due to the velocity over the wing becoming high enough to retard the change in circulation following control displacement. Under these conditions, the hinge moment acts in the direction of the motion for more than one-half a complete cycle so that a steady oscillation may exist. From the analysis it is concluded that controls must be designed with a large mass moment of inertia or with a high degree of irreversibility if damping is not used. When a mechanical restraining effect is in the control system, care must be taken in design of the control system to insure that the natural frequency of the system is not in the range of frequencies between one-half the aerodynamic frequency and the aerodynamic frequency.

INTRODUCTION

Tests of a full-scale partial-span airplane wing were undertaken in the 16-foot high-speed wind tunnel after an airplane employing this wing exhibited control-surface vibrations which were associated with high-speed flight (reference 1). The vibration was satisfactorily duplicated in the wind tunnel and was demonstrated to be a new type of flutter which is the result of the flow velocities in flight at high subsonic speeds. Because the flutter could not be prevented by restraining the motion of the wing in bending and torsion, it was

concluded that the surface could maintain steady or divergent oscillations about its hinge line with only one degree of mechanical freedom, which proved the existence of a new type of flutter. Flutter was prevented by restraining the control cables, producing a condition which simulates irreversible controls. Damping in the system was also effective in eliminating all but transient oscillation.

Several useful testing techniques were used. These consisted of (a) measuring the aerodynamic forces directly by the use of instantaneous recording pressure cells, (b) measuring the viscous damping required to prevent the flutter, and (c) photographing the shock wave motion and aileron motion by the use of shadowgraphs and measuring the phase difference between these motions. With the last arrangement a number of changes to the aerodynamic characteristics were investigated. This report is concerned primarily with the results of this investigation. Control-surface flutter is discussed and certain inferences as to other types of possible transonic flutter are indicated.

SYMBOLS

The symbols used in this report are defined as follows:

a	velocity of sound, feet per second
b_a	aileron span, feet
c	wing chord, feet
$\overline{c_a^2}$	mean-square chord of aileron, square feet
d	distance between shock wave and trailing edge, feet
f_a	aerodynamic frequency, cycles per second
f	flutter frequency, cycles per second
g	acceleration due to gravity, feet per second squared
m	mass, pound second squared per foot
q	dynamic pressure, pounds per square foot
s	distance from hinge line to center of gravity, feet
t	time, seconds

x	distance from leading edge, feet
A	variation of hinge moment with aileron angle $(\partial H/\partial \delta_{a_o})$, foot-pounds per radian
C	damping coefficient, foot-pounds per second
C_{h_a}	aileron hinge-moment coefficient $\left(\frac{H}{q b_a c_a^2}\right)$
ΔC_{h_a}	increment in hinge-moment coefficient due to buffeting
H	hinge moment, foot-pounds
H_o	amplitude of hinge-moment function, foot-pounds
I	aileron mass moment of inertia about the hinge line, foot-pounds seconds squared
K_m	equivalent spring constant, foot-pounds per unit angular displacement
M	free-stream Mach number
M_{cr}	critical Mach number
T	period of oscillation, seconds
α	angle of attack, degrees
δ_a	aileron angle, degrees or radians
δ_{a_o}	aileron angular amplitude, degrees or radians
Φ	phase angle between aileron displacement and shock displacement, degrees (Positive values indicate a lagging shock.)
Φ'	phase angle between aileron displacement and hinge moment, degrees (Positive values indicate a leading hinge moment.)
ω	flutter circular frequency $(2\pi f)$, radians per second
ω_a	aerodynamic circular frequency $(2\pi f_a)$, radians per second

TEST APPARATUS AND PROCEDURE

The test wing was a full-scale partial-span production wing of a fighter airplane and was mounted in the Ames 16-foot high-speed wind tunnel as shown in figure 1. The control surface, an aileron, had no aerodynamic balance and was hinged along the upper surface of the wing by a continuous piano-type hinge. For most of the tests the tip of the wing was supported in order to eliminate wing bending and torsion as nearly as possible (fig. 1).

The test wing had the following geometric characteristics:

Wing section	NACA 651-213, a = 0.5
Wing area	44.2 sq ft
Aileron area	8.75 sq ft
Wing span	9.85 ft
Mean aerodynamic chord	4.83 ft
Aileron span	7.5 ft
Aileron root chord	1.458 ft
Aileron tip chord	0.875 ft
Aileron root-mean-square chord	1.18 ft
Aileron hinge-line location	25 percent of wing chord from trailing edge

All instantaneous records were obtained on recording oscillographs. Hinge moments were measured by the use of electric strain gages. The aileron angle was recorded on the oscillographs through the use of potentiometers, and the wing motion was recorded by displacement pickups.

The principal data were obtained by using the shadowgraph system shown in figure 2. The point source of light should have been at the intersection of the projected straight-line wing elements, but in this particular case it was necessary that the source be closer to the wing; consequently, a shadow of the wing was cast on part of the screen. The light source was a Bol, high-pressure, mercury-vapor lamp which was operated on direct current so that high-speed motion pictures of the moving shock wave and aileron could be taken. The screen was the tunnel wall painted white. Black lines were painted

on the screen at the leading edge, 50 percent chord, and trailing edge so that the shock-wave positions could be measured. The light intensity limited, to approximately 100 frames per second, the camera speed at which data could be obtained. At this speed approximately five pictures were taken during each cycle of motion.

In obtaining the shadowgraphs, the aileron was restrained at an angle near zero, the tunnel speed was increased to that at which data were desired (approximately 0.81 Mach number), the camera was started, and then the aileron was released. In this manner pictures of the shock wave with and without aileron motion were obtained.

The Ames 1- by 3½-foot transonic wind tunnel was used for two short tests. In these tests the schlieren apparatus with a stroboscopic light was used to visualize the flow. The models for this wind tunnel were made of solid steel and spanned the test section.

RESULTS

Study of high-speed shadowgraphs of the aileron and shock-wave motions showed that consistent relationships between these motions could be measured, and indicated that useful information concerning the time lags in the flow changes about the wing could be obtained. The following paragraphs point out the significant results obtained for various modifications based, for the most part, upon shadowgraph data such as those presented in figures 3 through 24.

Standard Wing and Aileron

The photographs shown in figures 3 and 4 are consecutive pictures taken from a motion picture. In the first set (fig. 3), the relative steadiness of the shocks before the control was released is illustrated. In figure 4 are eight pictures illustrating the motion of the shock and aileron during flutter. By analyzing a series of these consecutive pictures (of which the eight shown were typical), the shock motion and corresponding aileron motion were determined.

In figure 5 the aileron and shock motion are plotted with the second and all subsequent cycles shifted to make them coincide with the first cycle. The data are approximated by sinusoidal curves which are also shown. The oscillograph records of the aileron position, taken at the same time as the motion pictures, were used to determine the amplitude and mean angle of the control in addition to the exact flutter frequency. The aileron angles are plotted with reference to the mean control angle. Figure 5 shows the time lag between the aileron position and the shock position and, therefore, the phase relation between the flow changes and the aileron motion.

It is to be noted that for the standard wing and aileron a phase difference of 67° existed between the shock motion and the aileron motion. The aileron motion was from 6.2° to −12.2°, a total motion of 18.4°, with a corresponding shock motion from 59.7 to 76.8 percent of the chord, a total motion of 17.1 percent. The noteworthy results for the other configurations are called to attention in the following paragraphs.

Spoilers at 50 Percent Chord, Upper and Lower Surface

The spoilers were installed in an attempt to fix the shock position by a local low-pressure area. The spoiler heights were 0.0030 and 0.0024 of the mean aerodynamic chord on the upper and lower surfaces, respectively. As shown by the pictures (figs. 6 and 7), there were relatively steady shocks at the spoilers by additional shocks formed farther back and oscillated with the aileron motion. The aileron motion was from 2.3° to −4.3° or a total of 6.6°, corresponding to a total shock motion of 11 percent of the chord (74 to 63 percent). The phase difference (fig. 8) was 17°, substantially less than that with the standard wing.

Faired Bumps at the 50-Percent-Chord Position

Because the spoilers limited the flutter somewhat, it was decided that additional investigation of low-pressure areas was desirable. The first step was to fair over the spoilers with bumps of 6-inch chord. The relatively steady shocks at the midchord point were much less intense, and the double amplitude of the control flutter was the same as for the standard configuration (18.6°), although the motion of the shocks back of those on the bumps increased to a total of 27.5 percent of the chord (82.5 to 55.0 percent). (See figs. 9, 10, and 11.)

Faired Bumps at the 70-Percent-Chord Position

As it was not possible to fix the shocks at the 50-percent-chord position without another shock forming farther aft, faired bumps were added at the position where the shock motion for the standard wing centered, at 70 percent of the chord. Bumps on each surface were designed to have lower critical Mach numbers than the 50-percent-chord point of the standard wing at an angle of attack of 1°. They had a chord of 6 inches and the heights were 0.0055 and 0.0032 of the mean aerodynamic chord for the upper and lower surfaces, respectively. The shock formation was not as clear-cut as for the standard case and a double shock appeared in some of the pictures. (See fig. 13.)

It is interesting to note that the shocks seemed to oscillate between the normal-peak-pressure points and the bump-peak-pressure points (fig. 14), although the significance of the forward motion of the center-of-shock oscillation is obscured in the fact that the angle of attack was inadvertently set at 1° for this test. The aileron motion was from 4° to −5° with a corresponding shock motion from 59.6 percent to 71 percent of the chord.

Variation of Thickness Ratio Along the Span

The percentage thickness of the wing was varied along the span by increasing the thickness by 2 percent of the chord at the inboard section and tapering to the original section at the tip. (See fig. 15.) Because only the upper surface was altered, a variation in camber also occurred. The increased thickness, combined with the increased camber, lowered the critical Mach number of the inboard section by about 0.05. The purpose of testing this configuration was to ascertain whether varying the critical Mach number along the span would affect the flutter. Flutter did result even though the variation in critical Mach number over the semispan was unusually large (from 0.68 to 0.72 for 51 percent of the semispan). The motion of the shock was reduced, being only from 58.8 percent to 67.5 percent of the chord (fig. 18) with a corresponding aileron motion from −10° to 6°, but the aileron motion was greater relative to the shock motion in this case as compared to the other cases. Tapering in thickness actually gave a greater aileron motion for a smaller indicated shock motion.

Vent Holes Between Upper and Lower Surface

In an attempt to control the flow over the aft part of the wing, circular holes were cut in the wing surfaces ahead of the hinge line, since the piano-type hinge did not permit flow between the upper and lower surfaces. Two tests were conducted: the first with holes in the upper surface only (figs. 19, 20, and 21) and the second with holes in both surfaces (figs. 22, 23, and 24). The results for both cases were about the same; the phase lag of the shock was greater than for any other condition. This increased lag can be explained by the fact that the flow through the holes was normal to the flow over the wing. The flow would normally tend to be from the unseparated to the separated side and probably increased the intensity of separation on one side and delayed the start of separation on the opposite side.

Aileron-Contour Change

The aileron contour was changed to a flat-sided, blunt-trailing-edge arrangement, changing the aileron trailing-edge angle to 12°. (See figs. 25 and 26.) This aileron fluttered in the same manner as the others except that the frequency was decreased to 15.9 cycles per second as a result of the increased inertia of the aileron.

Aileron Mass Overbalance

With the wing tip free, some motion of the wing occurred during transonic flutter, indicating that mass overbalance of the aileron might provide damping. The aileron was overbalanced by 29 percent with weights located as far outboard as possible. This overbalance had little effect on the flutter except to alter its frequency slightly.

Dampers

Hydraulic- and inertia-type dampers were found capable of preventing sustained oscillation, even though the damping capacity was small. Although the dampers prevented sustained oscillation, the ailerons still shook irregularly due to play in the systems tested.

Wing Flutter

During one of the first shadowgraph trials the tunnel speed was increased to 0.825 Mach number and the standard set of data was taken. Just as the camera ran through its film and the oscillograph was shut off, the violence of the motion in the tunnel increased greatly and the oscillograph operator took another record. These two records are shown in figure 27. The records of the aileron motion and wing motion are indicated. It is to be noted that the first record shows sinusoidal aileron motion at 20.6 cycles per second with wing motion at the same frequency but of small amplitude. The changed motion is evident in the next record where the wing motion was sinusoidal at 13 cycles per second and the aileron motion was erratic. This shows a change from aileron flutter to wing flutter. The wing flutter was either the cause or the result of the wing failure shown in figure 28. It is probable that an initial failure of the structure due to aileron flutter reduced the restraint enough to allow the wing to flutter. The primary bending frequency of this wing in still air, before the failure, was about 15 cycles per second, slightly higher than that at which the flutter occurred.

Buffeting Forces on Fixed Controls

It was found that with the control held as rigidly as possible there were still rather large buffeting forces present although the flutter was eliminated. Figure 29 is from records obtained during buffeting. The sharp breaks in the records of aileron position were caused by dirt particles on the slide wire. The aileron was being held very steady until the highest Mach numbers were reached. Several such records were analyzed to obtain the average amplitudes and frequencies of buffeting shown in figure 30. The frequency of buffeting at all Mach numbers was approximately 32 cycles per second. At 0.825 Mach number, the force variation was so large that holding the aileron absolutely steady became extremely difficult, and the motion apparently included higher harmonic content plus a beating effect all superimposed on a 3-cycle-per-second oscillation.

The buffeting hinge-moment coefficients from figure 30 for this wing and aileron seem to vary linearly with Mach number so that

$$\frac{\Delta C_{h_a}}{\Delta M} = 0.113 \qquad (1)$$

The figure shows that ΔM was equal to M-0.73. The Mach number 0.73 is approximately the critical Mach number of this section.

Static Characteristics

The static hinge-moment data (fig. 31) show no unusual reversals of hinge moment. The only compressibility effect noted is a slight increase in $\partial C_{h_a}/\partial \delta_a$ with increasing Mach number.

The drag data (fig. 32) are presented in conjunction with figure 33 to show that the lowest speed at which flutter could be induced was above the Mach number of drag divergence. The increase in drag between 0.5 and 0.7 Mach number was largely due to increasing tare drag. It can be seen that for this wing the flutter did not start until the drag coefficient had increased about 0.01 above its low-speed value.

DISCUSSION

Interpretation of Test Results

The results of this test show that the flutter motion was sinusoidal and that a phase difference existed in the response of

the air flow about the wing relative to motions of the control. It has also been shown that the amount of this phase difference, as indicated by the shock waves, can be measured.

The phase difference referred to is the phase difference between the relative motions of the shocks and the aileron. (See figs. 5, 8, 11, 14, 15, 21, and 24.) This phase angle is called a lagging angle on the basis that an upward motion of the control caused a forward movement of the shock. The hinge moment during flutter is associated with control movement in the same manner as with fixed control positions, except for the phase difference in the response of the hinge moments to control movements, as indicated by the lagging shock motion. The effect of this lag in causing flutter can be explained by considering an example in which there is a lag in the shock motion of one-eighth of a cycle or 45°. The hinge moment would then be maximum when the aileron is moving in the down (positive) direction and is halfway between the mean and the maximum negative angle. This hinge moment would then be in the direction of the motion for 270° or three-quarters of the total cycle. Therefore, positive work would be done and, unless sufficient damping were present, a divergent vibration would occur. Preliminary computations can now be made using the phase angles measured from the shadowgraphs.

The familiar mathematical representation of the one-degree-of-freedom system which will be used in this report follows. The differential equation of motion with a sinusoidal forcing function, inertia, damping, and spring restraint is

$$I\ddot{\delta}_a + C\dot{\delta}_a + K_m\delta_a = H_o \sin \omega t \qquad (2)$$

In the tests reported herein the aileron was free from elastic restraint, and the gravity forces were estimated to be less than 1 percent and are considered negligible. Under these conditions equation (2) becomes

$$I\ddot{\delta}_a + C\dot{\delta}_a = H_o \sin \omega t \qquad (3)$$

Letting the displacement

$$\delta_a = \delta_{a_o} \sin (\omega t + \Phi')$$

then

$$\dot{\delta}_a = \delta_{a_o} \omega \cos (\omega t + \Phi')$$

CONFIDENTIAL

$$\ddot{\delta}_a = -\delta_{a_o} \omega^2 \sin (\omega t + \Phi')$$

substituting this solution in (3)

$$-I\delta_{a_o}\omega^2 \sin(\omega t + \Phi') + C\delta_{a_o}\omega \cos(\omega t + \Phi') = H_o \sin \omega t \qquad (4)$$

For steady conditions

$$I\delta_{a_o}\omega^2 = -H_o \cos \Phi' \qquad (5)$$

and

$$C\delta_{a_o}\omega = -H_o \sin \Phi' \qquad (6)$$

where Φ' is the phase difference between the hinge moment and the aileron position as measured from the shadowgraphs. From the above equations, it follows that

$$H_o = \delta_{a_o}\ \omega\,(C^2 + I^2\omega^2)^{\frac{1}{2}} \qquad (7)$$

where H_o is the magnitude of the resultant aerodynamic vector moment.

Analysis of Results

In table I a summary of the data obtained from the shadowgraphs is presented, and the aerodynamic vector magnitudes and phase positions are listed. The shock phase difference (column 5) was reduced by 33 ← percent to conform with pressure measurements made with the standard configuration which accounts to some extent for the differences noted in table II. The corrected phase was used in computing the values in column 8. Column 8 indicates a linear variation of the aerodynamic hinge moment with aileron displacement during flutter and is referred to as the dynamic slope in this report.

The static results (fig. 31) for the standard wing and aileron indicate that the average static variation of the hinge moment with aileron angle agrees closely with the dynamic variation indicated in table I. It is recommended, for the present, that the dynamic hinge moments be assumed equal to the static hinge moments in the analysis of transonic flutter. It must be noted that low-speed hinge-moment slopes will generally not be satisfactory because of the large changes possible with transonic flow.

If the static hinge moments are always an indication of the dynamic effect, then aerodynamic balance will reduce the dynamic hinge moments during transonic flutter. Table I shows also that when separation was forced to occur at the 50-percent-chord point the flutter was less severe due probably to the decreased hinge-moment slope.

Method for Treating the Transonic Flutter Problem

In order to solve the transonic flutter problem in the same manner as the low-speed flutter problem is solved, it is necessary to be able to compute the frequency at which flutter will occur, the phase angle of the driving hinge moment, and the magnitude of this hinge moment.

The method presented uses the real or in-phase component of the aerodynamic hinge moment under static conditions as a means of estimating the magnitude of the resultant dynamic hinge moment. The method assumes a linear variation of hinge moment and, although this assumption may be improved later, it is believed that the recommended method of design should be satisfactory. The mechanical oscillation theory indicates that flutter with one degree of freedom can result from a time lag in the changes of the flow about the wing. The time lag can be accentuated when the velocity over the wing approaches the speed of sound. Impulses from the trailing edge travel forward at a speed equal to the speed of sound minus the local airspeed. A study of the various methods by which the impulses might propagate indicates that the controlling time lag is probably that time required for a pressure impulse from the trailing edge to reach the shock position. It then is necessary to determine this time lag in terms of the local velocity over the wing.

Static pressure-distribution data for airfoil sections at transonic speeds show that the local velocity aft of the shock drops to a value near sonic velocity and leaves the trailing edge at approximately the free-stream velocity. Assuming that impulses from the trailing edge propagate forward at the speed of sound minus the local velocity outside the boundary layer, the time for the impulses to reach the shock position, assuming linear variations of local velocity, is

$$\text{Time} = \frac{K2d}{a(1-M)}$$

where

d the distance from the trailing edge to the shock

M the free-stream Mach number

a the velocity of sound

The factor K is inserted in the equation to account for the additional time required for the complete change to take place in the flow about the wing. This constant was estimated as being approximately equal to two. This value of the constant is inserted and the equation is inverted and used in terms of a frequency as follows:

$$f_a = \frac{a(1-M)}{4d} \tag{8}$$

The parameter f_a will be called the aerodynamic frequency. This formula indicates the frequency at which steady aerodynamic oscillations, if any, would occur. In an effort to check the formula, the buffeting frequencies that occurred with no detectable aileron motion were investigated. From figure 34 it can be found that at 0.75, 0.78, and 0.82 Mach number the steady shocks for an angle of attack of -1° and an aileron angle of 0° are, respectively, at 53, 63, and 67 percent of the chord; the corresponding aerodynamic frequencies calculated from equation (8) are 31.3, 31.8, and 31.2 cycles per second, respectively. A chord equal to the average wing chord at the aileron (4.67 ft) was used in the calculations. These values provide satisfactory agreement with the measured frequency of buffeting, which was approximately 32 cycles per second. The following phase angle equation is based on an upper flutter limit equal to the aerodynamic frequency and a lower flutter limit based on experimental data which indicate that damping begins to be negative at one-half the aerodynamic frequency. It should be recognized that incipient vibrations could appear near this assumed lower limit.

$$\Phi' = \left(1 - \frac{f}{f_a}\right)360 \tag{9}$$

where f is the flutter frequency, and f_a is the aerodynamic frequency as determined from equation (8). In order to check this equation against the results obtained by the shadowgraphs, table II was prepared. The aerodynamic frequency was computed using the average position of the shock during flutter.

[redacted]

Table II shows considerable variation in some individual results but the average values are only 11° apart, which is considered to be quite good. The individual values cannot be used independently because the fairing of the harmonic approximations could be altered in some cases; therefore, the average of all the cases is considered a better check point.

Additional Data Substantiating the Aerodynamic-Frequency and Phase-Angle Formulas

Transonic tests of two small two-dimensional airfoils (6- and 8-inch chords) have been conducted in the Ames 1- by 3½-foot transonic wind tunnel. The data obtained to date are meager but tend to substantiate the aerodynamic frequency and phase-angle formulas. For the 8-inch-chord airfoil:

(a) The shock formed approximately 3 inches from the trailing edge at 0.875 Mach number.

(b) Flutter was divergent at approximately 100 cycles per second.

The phase angle is determined by using the fact that the natural frequency was nearly the same as the flutter frequency, approximately 100 cycles per second. In any system with only one degree of freedom operating at or near its natural frequency, the forcing vector will be at or near 90°. It was found that, by using 90° as the phase relation, the aerodynamic frequency would be 134 cycles per second (equation (9)). From equation (8) the predicted aerodynamic frequency would be 137 cycles per second, which checks the experimental value very well.

The second small-scale experiment involved a rigid wing without a hinged control surface. This condition can be assumed to be equivalent to a wing or tail with a rigidly fixed control surface. The rigidity was such that no detectable motion of the model was noted although the shock waves oscillated over about 20 percent of the chord. The following results were obtained:

(a) The shock wave appeared approximately 4.5 inches from the trailing edge at 0.675 Mach number.

(b) The shock oscillated at approximately 250 cycles per second.

This is a condition similar to the buffeting with fixed controls and the aerodynamic frequency (from equation (9)) must equal the flow-oscillation frequency of 250 cycles per second. Computing the

aerodynamic frequency for conditions (a) by equation (8) gives 240 cycles per second, again a satisfactory check with the experimental data.

It is believed that the excellent correlation between the test results and the suggested empirical equation for predicting the aerodynamic frequency justifies its use until a more rational solution is developed.

Applying the Suggested Solution to the General Case

It has been shown that the method presented for determining the phase angle gives results which agree with the data available; therefore, the computed frequency can probably be used to establish design criteria for other airfoils and controls. In computing the aerodynamic frequency up to this point the position of the shock has been determined from shadowgraphs. A method of estimating the shock position is required because shadowgraph data will not, in most cases, be available. It is recommended that the distance to the point of minimum pressure and the critical Mach number of the section be used in computing the aerodynamic frequency f_a. For example, the minimum pressure on the standard wing tested was at 50 percent of the chord, and the theoretical critical Mach number is 0.72. With these values and the average chord, the aerodynamic frequency is 33 cycles per second. This frequency is in close agreement with the 32 cycles per second calculated from the actual static shock position and Mach number, and with the 35 cycles per second calculated frequency from the mean position of the shock during flutter. It is to be noted that the phase angle for the wing with tapered thickness (114°) calculated from the mean shock position and the Mach number during flutter does not check the angle measured by the shadowgraph method (155°). Computing this phase angle by using the critical Mach number and the minimum pressure point as suggested involves using an average critical Mach number, due to the taper in thickness, which was about 0.695. The minimum pressure was still at the 50-percent-chord point and, as a result, the computed phase angle is 152°, which is close to the 155° determined from the shadowgraphs.

The solution of the equation for the system with one degree of freedom has been presented for the system having zero spring effect. In applying the analyses to control surfaces, there will usually be a spring restraint resulting from the control cables and structural deformation. The steady-state solution for this case when the spring force opposes the displacement is

$$\delta_{a_o} = \frac{H_o}{\left[(C\omega)^2 + (K_m - I\omega^2)^2\right]^{\frac{1}{2}}} \qquad (10)$$

[redacted]

Assuming a constant variation of dynamic hinge moment with aileron angle,

$$l = \frac{A}{[(C\omega)^2 + (K_m - I\omega^2)^2]^{\frac{1}{2}}} \tag{11}$$

If the absolute magnitude of this ratio is greater than one, divergence will tend to occur, if less than one, convergence. Therefore, the condition for preventing steady flutter is

$$[(C\omega)^2 + (K_m - I\omega^2)^2]^{\frac{1}{2}} > A \tag{12}$$

and

$$\tan \Phi' = \frac{C\omega}{(K_m - I\omega^2)} \tag{13}$$

The phase angle, equation (9), is

$$\Phi' = \left(1 - \frac{f}{f_a}\right) 360$$

and, therefore, the frequency of oscillation will be

$$\frac{\omega}{2\pi} = f = \frac{f_a}{360}\left[-\tan^{-1}\left(\frac{C\omega}{K_m - I\omega^2}\right) + 360\right] \tag{14}$$

When K_m is smaller than $I\omega^2$, the oscillation frequency is between $0.5\ f_a$ and $0.75\ f_a$, and when K_m is greater than $I\omega^2$, the frequency is between $0.75\ f_a$ and f_a. If the two quantities are equal or

$$(0.75\ f_a\ 2\pi)^2\ I = K_m$$

a resonant condition exists and the large amplitudes associated with resonance can be expected. In the appendix, specific design considerations are discussed.

CONCLUSIONS

The data that have been presented in this report show that control-surface flutter can result from transonic flows due to the time lag in the flow changes about the wing. The following general conclusions can be made:

1. The results and analysis of the tests discussed have indicated that transonic flutter can be prevented by any of the following methods:

   (a) An irreversible control system. If this system is used it should be rigid enough so that the natural frequency of the system is greater than the aerodynamic frequency.

   (b) A high inertia control system. With this system the elastic restraint must be a minimum (natural frequency less than one-half the aerodynamic frequency), and the inertia will generally be much greater than that resulting from conventional design.

   (c) Addition of mechanical damping. Mechanical damping will generally be required if the natural frequency of the system is between one-half the aerodynamic frequency and the aerodynamic frequency. In some cases, mechanical damping may be used in combination with either (a) or (b).

   (d) Aerodynamic balance. The only balance that can be considered as being effective would be the overhanging type, either internal or external.

2. A method of analysis has been suggested which appears to have some merit and it is recommended for general use until more exacting solutions are developed.

3. Even when flutter is prevented, there are indications that buffeting at the aerodynamic frequency may be experienced.

4. It appears, on the basis of the suggested solution, that wing section will affect flutter primarily by its control of the location of the shock, except that, regardless of section contour,

increasing the critical Mach number of the section will decrease the range of Mach numbers in which transonic flutter will occur.

Ames Aeronautical Laboratory,
National Advisory Committee for Aeronautics,
Moffett Field, Calif.

APPENDIX

DESIGN CONSIDERATIONS

Mechanical Considerations

The aileron used for the tests described in this report had a mass moment of inertia of 0.4083 foot-pounds seconds squared. Assuming zero damping and no spring restraint, it is found from equation (14) that

$$f = 0.5\, f_a$$

therefore

$$I(2\pi f)^2 = 4390$$

The dynamic hinge-moment slope was -163 foot-pounds per degree or approximately -9300 foot-pounds per radian (table I). Therefore, the inertia would have to be more than doubled or damping would have to be added to prevent sustained flutter because the ratio (equation (11)) would be 2.1 instead of less than one as required. If it is not feasible to increase the inertia of the system or to add damping, the only other alternative would be to restrain the aileron and make its natural frequency very high. The spring constant required can be computed assuming $I\omega^2$ less than K_m and $C\omega^2$ equal to zero in equation (14);

$$f = f_a$$

then using equation (12),

$$[\, I(2\pi f_a)^2 - K_m]^2 > - 9300^2$$

$$I(2\pi f_a)^2 = 17{,}600$$

so K_m must equal 26,900 foot-pounds per radian at least, and the natural frequency of the system must be 41 cycles per second or more. In both cases that have been considered, zero damping has been assumed. Actually there will always be some damping in the

system from working of the structure, friction, and aerodynamic sources. Unless it is found or estimated that this inherent damping is large, it should be used as a margin of safety.

Variation of the Aerodynamic Frequency

The preceding discussion has considered the problem of preventing flutter by proper mechanical design of the control surface. It is interesting to consider the possibility of changing the shape of the wing so that the aerodynamic frequency is high enough or low enough so that flutter will not occur with the existing mechanical conditions. For example, if it were desired to use the inertia of the system (0.4083 ft-lb sec^2) to prevent flutter, assuming zero damping and no spring restraint, equation (12) requires that

$$I\omega^2 > 9300$$

therefore

$$f > 24 \text{ cycles per second}$$

and from equation (14)

$$f_a > 48 \text{ cycles per second}$$

The aerodynamic frequency for the test wing can be increased to the required 48 by any one of three methods or by combinations of these methods. These are (a) reducing the average chord to 3.20 feet without altering the airfoil section, (b) altering the section so as to move the peak pressure aft to 65.6 percent of the chord, or (c) reducing the critical Mach number to about 0.60 by making the section thicker. The only solution of any practical significance is probably the one wherein the peak pressure is moved aft; however, even this solution has some objections.

In the case of an irreversible control, the natural frequency must be high and the aerodynamic frequency should be lowered rather than increased.

Effect of Spanwise Variation of Aerodynamic Frequency

The final design condition to be considered is the variation of the aerodynamic frequency along the span. Due to the changes in the distance from the shock wave to the trailing edge and/or variation of the critical Mach number along the span, a variation in the phase relation of the forces along the span can be produced. In all the calculations the average chord over the aileron has been used in calculating the phase relation of the resultant force. The agreement with available experimental data has confirmed the validity of this assumption. It is advisable to investigate the effect of the variation of phase angle along the span of the control surface if there is a possiblity of a large variation. When the change in phase angle approaches 360°, torsional loading and torsional vibrations may become important. If f_{a_1} and f_{a_2} are the aerodynamic frequencies at the inboard and outboard ends of the aileron, respectively, the frequency at which the 360° variation occurs is

$$f = \frac{f_{a_1} f_{a_2}}{f_{a_2} - f_{a_1}}$$

From the above equation it can be shown that the variation in the distance from the shock to the trailing edge over the span of the aileron at a given flutter frequency must be

$$d_1 - d_2 = \frac{a\,(1 - M)}{4f}$$

For example, with a flutter frequency of 20 cycles per second $d_1 - d_2$ must equal 3.84 feet to obtain 360° phase variation across the aileron span. This variation has not been checked experimentally; however, it is definitely possible that combinations of high taper ratio and considerable aerodynamic balance would prevent flutter due to the variation along the span mentioned and the reduced hinge moments. Of course, the inertia of the control and the type of restraint, if any, also enter into the picture. Although the considerations just discussed may help to explain why certain configurations do not flutter it is obvious that these considerations cannot be utilized in a design at the present time due to many other factors involved.

REFERENCE

1. Brown, Harvey H., Rathert, George A., and Clousing, Lawrence A.: Flight-Test Measurements of Aileron Control-Surface Behavior at Supercritical Mach Numbers. NACA CRM No. A7A15, 1947.

TABLE I.- SUMMARY OF SHADOWGRAPH RESULTS

Configuration	1 Shock position (percent c)		2 Shock displacement (percent c)	3 Aileron angle (deg)		4 Aileron motion total (deg)	5 Phase difference Φ (deg)	6 Frequency f (cps)	7 Maximum hinge moment H_o (ft-lb)	8 Unit hinge moment $\left(\frac{\text{ft-lb}}{\text{deg}}\right)$
	Minimum	Maximum		Minimum negative	Maximum positive					
Standard	59.7	76.8	17.1	12.2	6.2	18.4	67	21.2	1500	-163
Spoilers at 0.50c	63	74	11.0	4.3	2.3	6.6	17	19.5	360	-109
Bumps at 0.50c	55	82.5	27.5	11.3	7.3	18.6	51	21.2	1362	-147
Bumps at 0.70c	59.6	71	11.4	5.0	4.0	9	54	19.4	570	-127
Tapered bump	58.8	67.5	8.8	10	6	16.0	25	20.8	1030	-128
Vent holes, upper surface	60	70	10.0	4.4	5.7	10.1	74	20.7	750	-182
Vent holes, upper and lower surfaces	61.8	70.4	8.6	5.1	5.4	10.5	73	21.2	1040	-198

M = 0.81 except for conditions 6 and 7 where M = 0.80.

$\alpha = -1^\circ$ except for condition 4 where $\alpha = 1^\circ$.

TABLE II.- COMPARISON OF COMPUTED PHASE ANGLES WITH THE VALUES DETERMINED FROM SHOCK POSITION

	1	2
Configuration	Phase angle from equation (9) (deg)	Phase angle from table I (deg)
Standard	142	113
Spoilers at 0.50c	153	163
Bumps at 0.50c	147	129
Bumps at 0.70c	144	126
Tapered bump	114	155
Vent holes, upper surface	139	106
Vent holes, upper and lower surfaces	141	107
Average	140	129

Average error, 11°

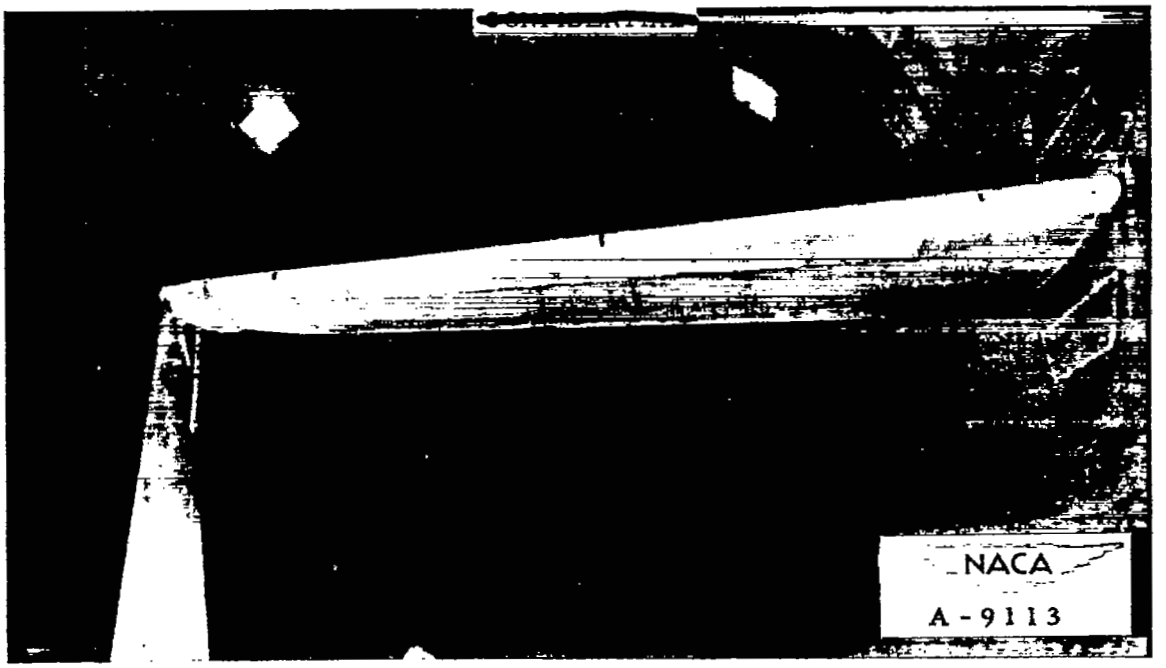

(a) General view of tip support.

(b) Detail of tip support.

Figure 1.- Partial-Span Wing.

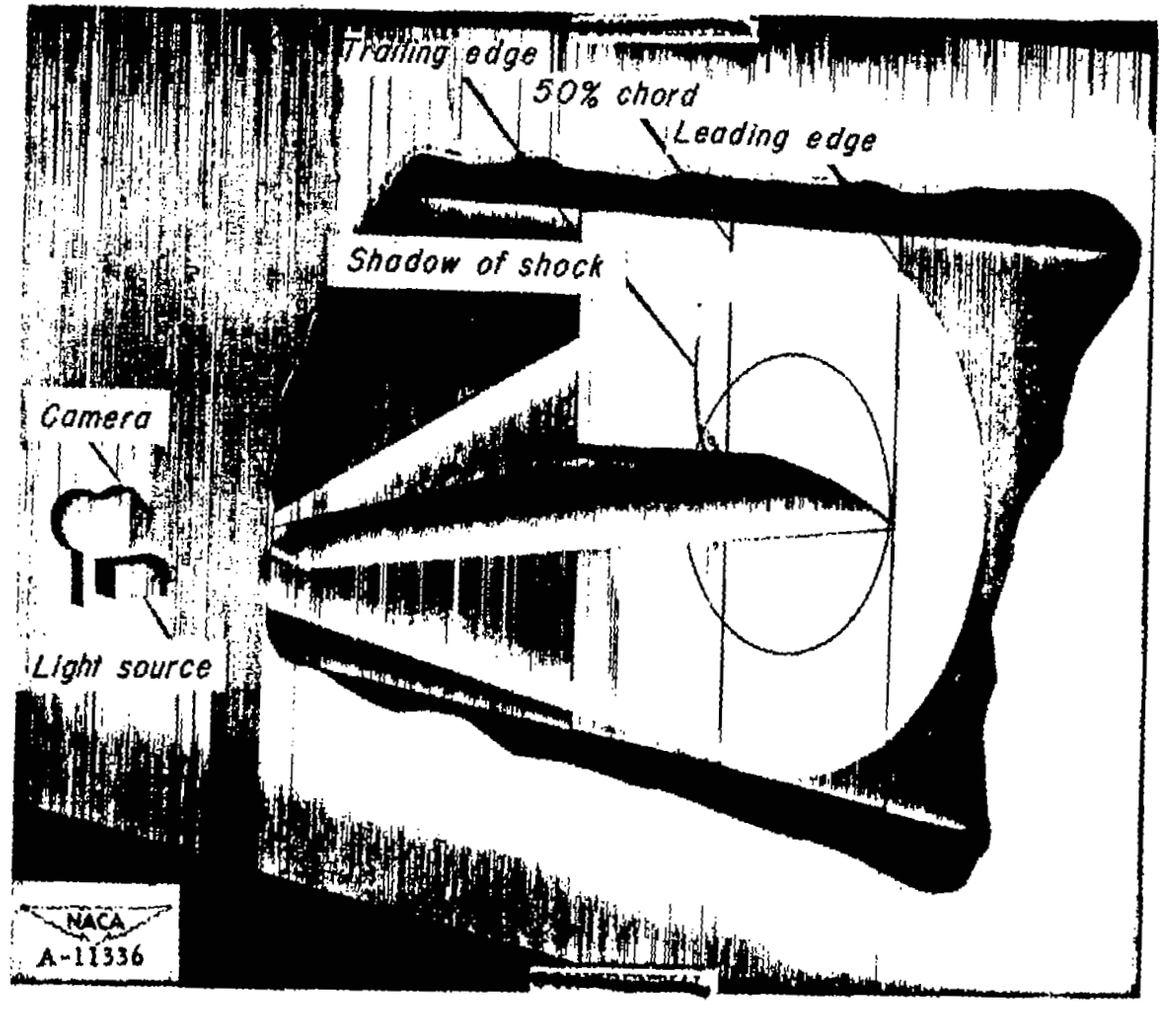

Figure 2. - Shadowgraph System

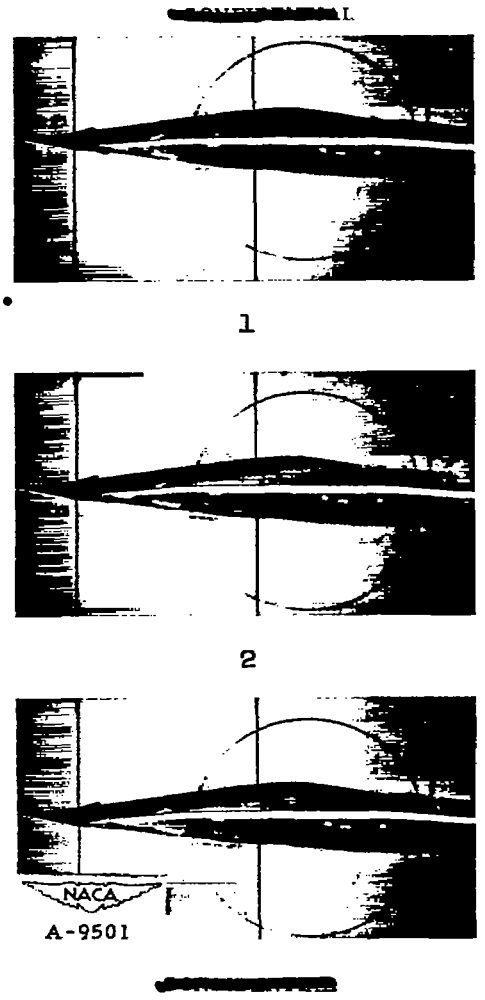

Figure 3. - Consecutive shadowgraphs of the wing with aileron fixed. Mach number 0.81; angle of attack -1°; standard configuration.

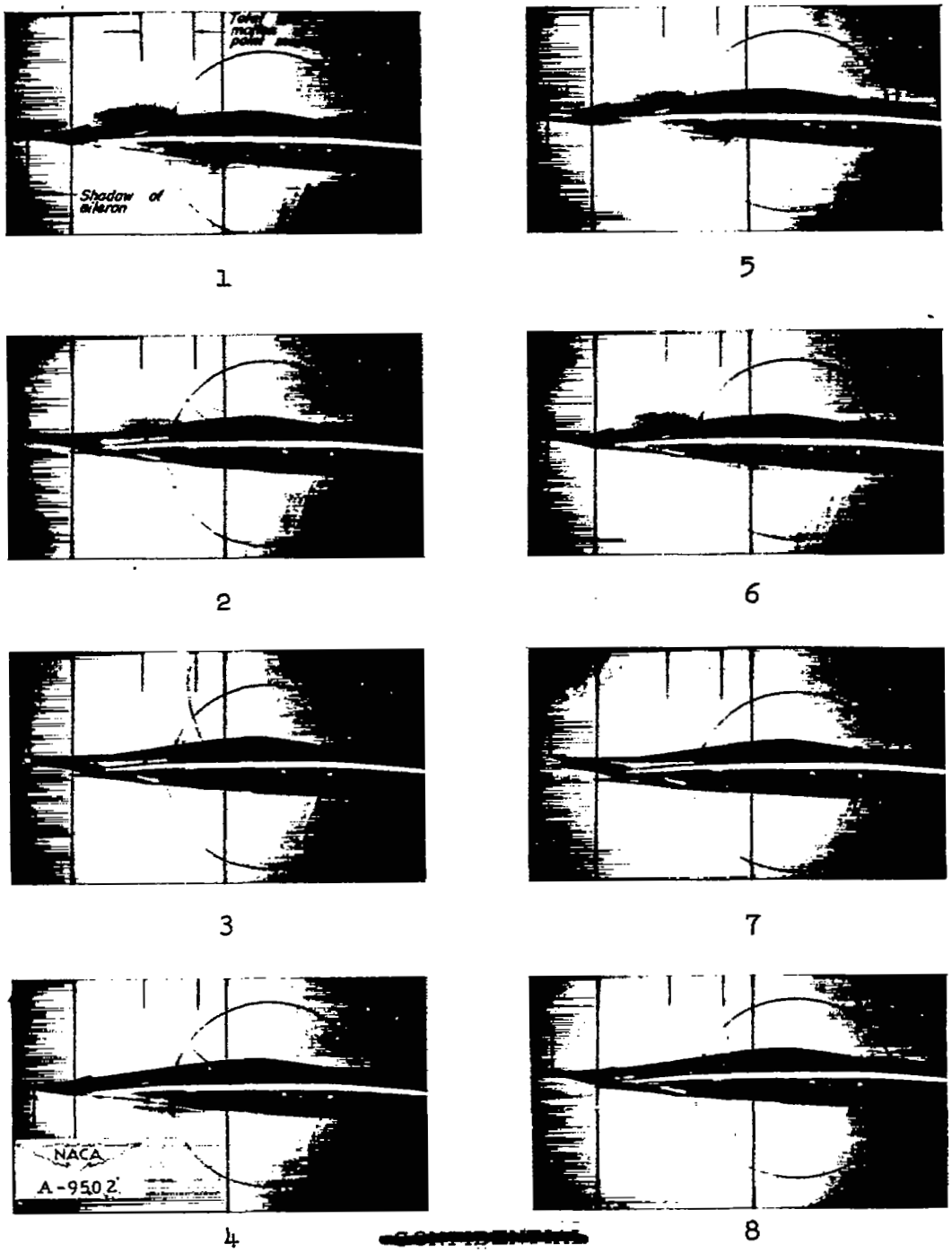

CONFIDENTIAL

Figure 4. - Shadowgraphs of the wing with the aileron free. Mach number, 0.81; angle of attack, -1°; standard configuration.

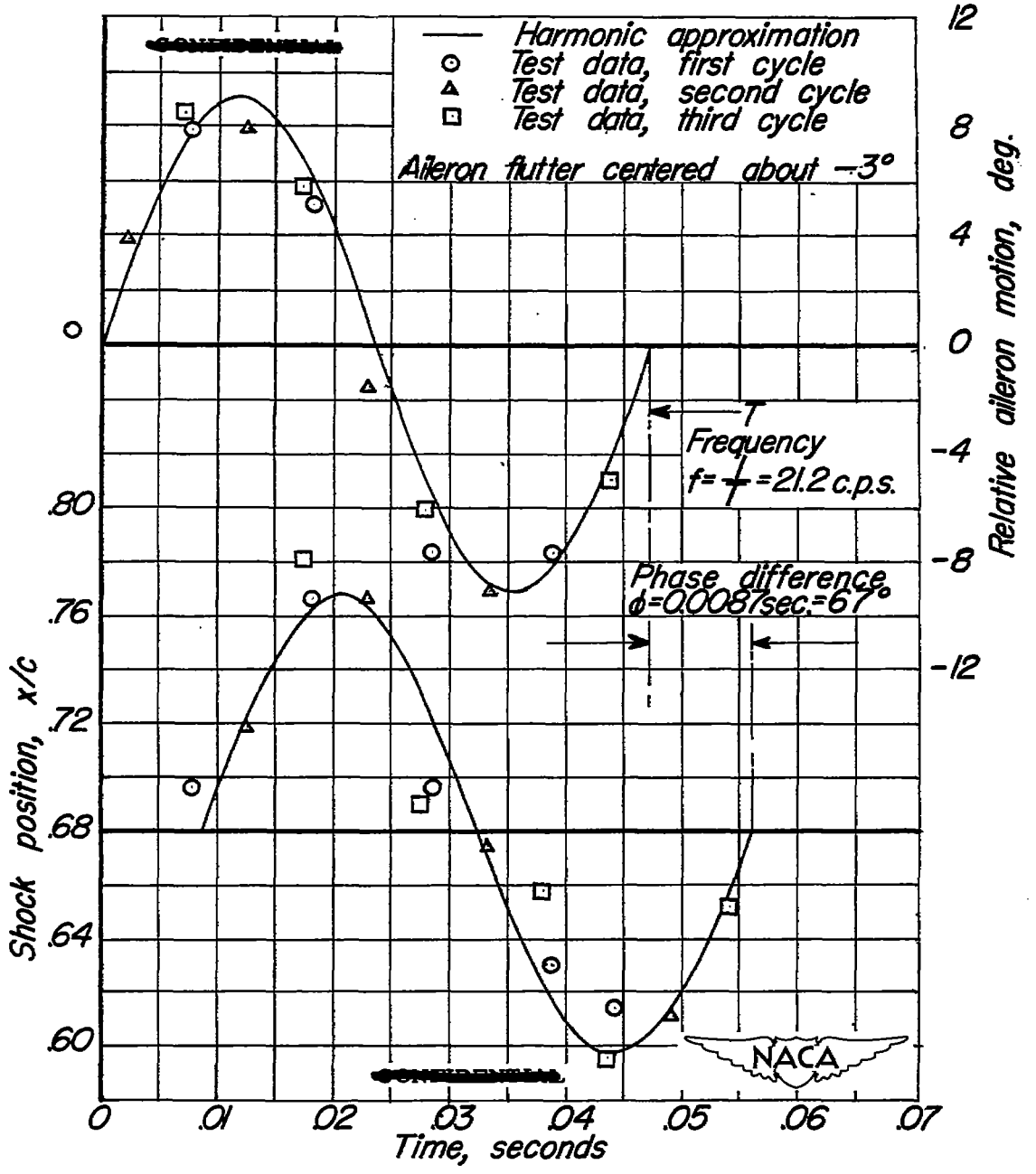

Figure 5.—Variation of aileron angle and normal shock position with time. Mach number, 0.82; angle of attack, −1°; standard configuration.

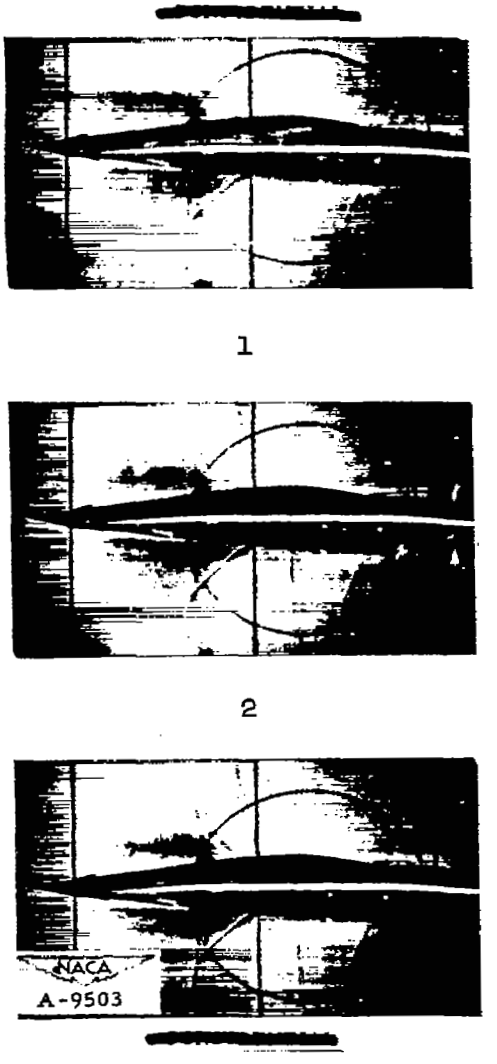

Figure 6. - Consecutive shadowgraphs of the wing with the aileron fixed. Mach number 0.81; angle of attack, -1°; spoilers at 50 percent chord on the upper and lower surfaces.

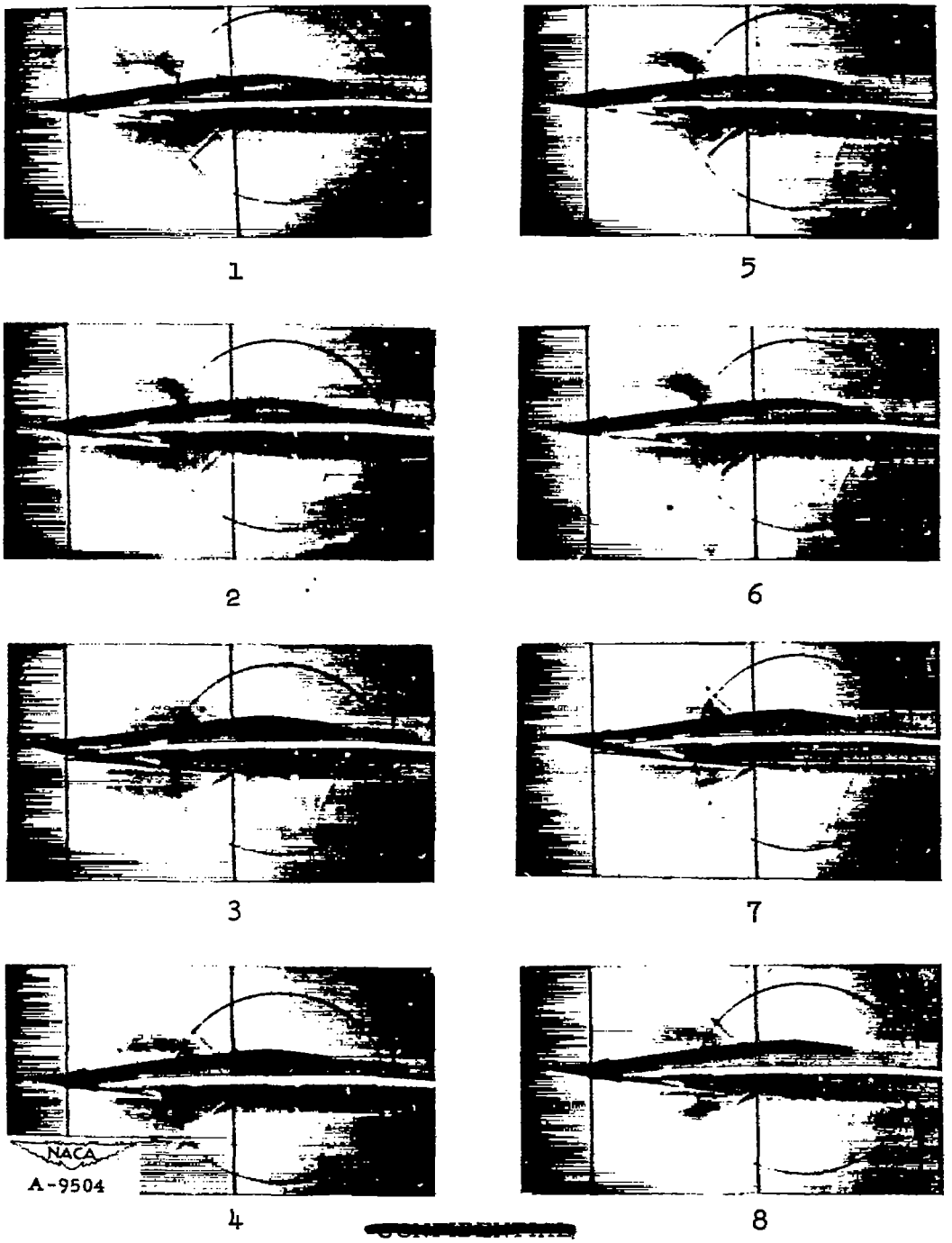

[redacted]

Figure 7. - Shadowgraphs of the wing with the aileron free. Mach number, 0.81; angle of attack, -1°; spoilers at 50 percent chord on the upper and lower surfaces.

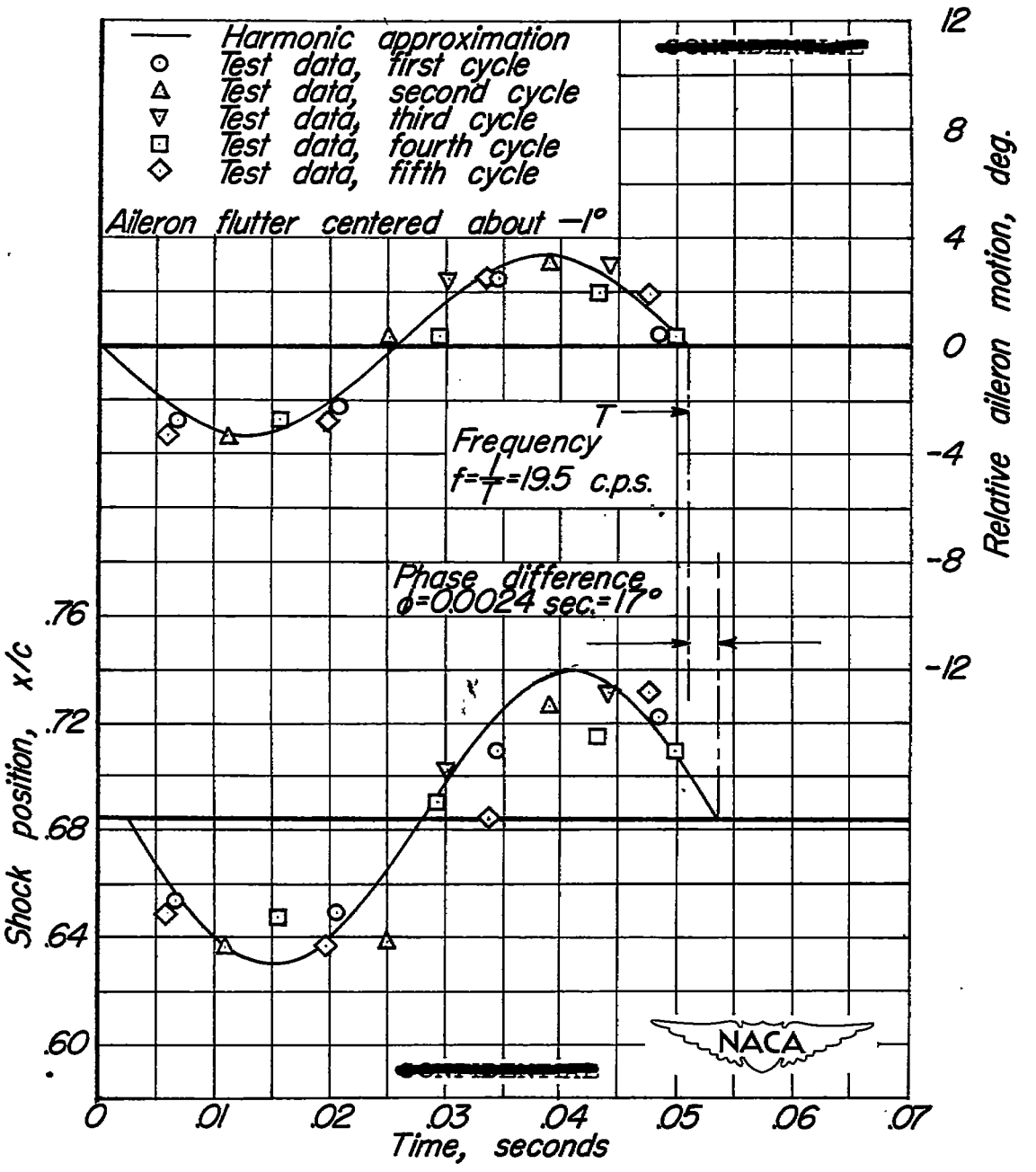

Figure 8.—Variation of aileron angle and normal shock position with time. Mach number, 0.81; angle of attack, −1°; configuration, spoilers at 50 percent chord on the upper and lower surfaces.

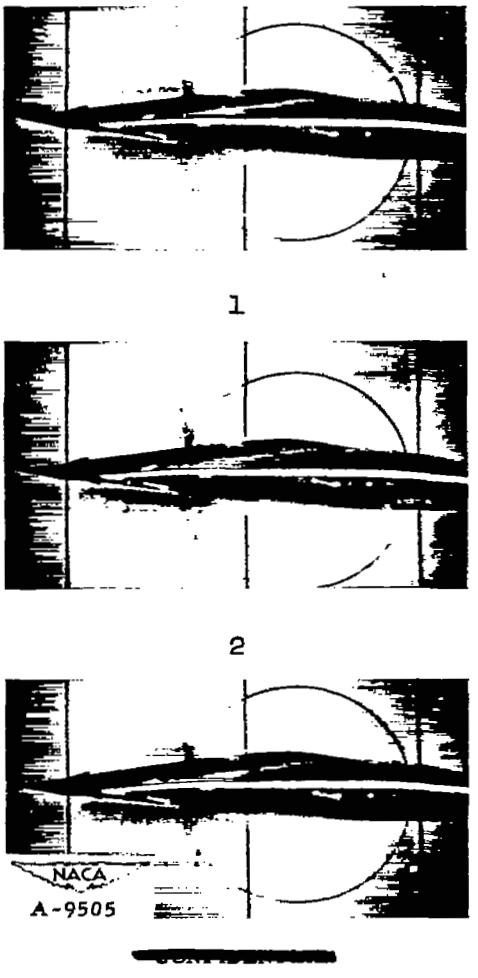

Figure 9.- Consecutive shadowgraphs of the wing with the aileron fixed. Mach number 0.81; angle of attack, -1°; faired bumps at 50 percent chord on the upper and lower surfaces.

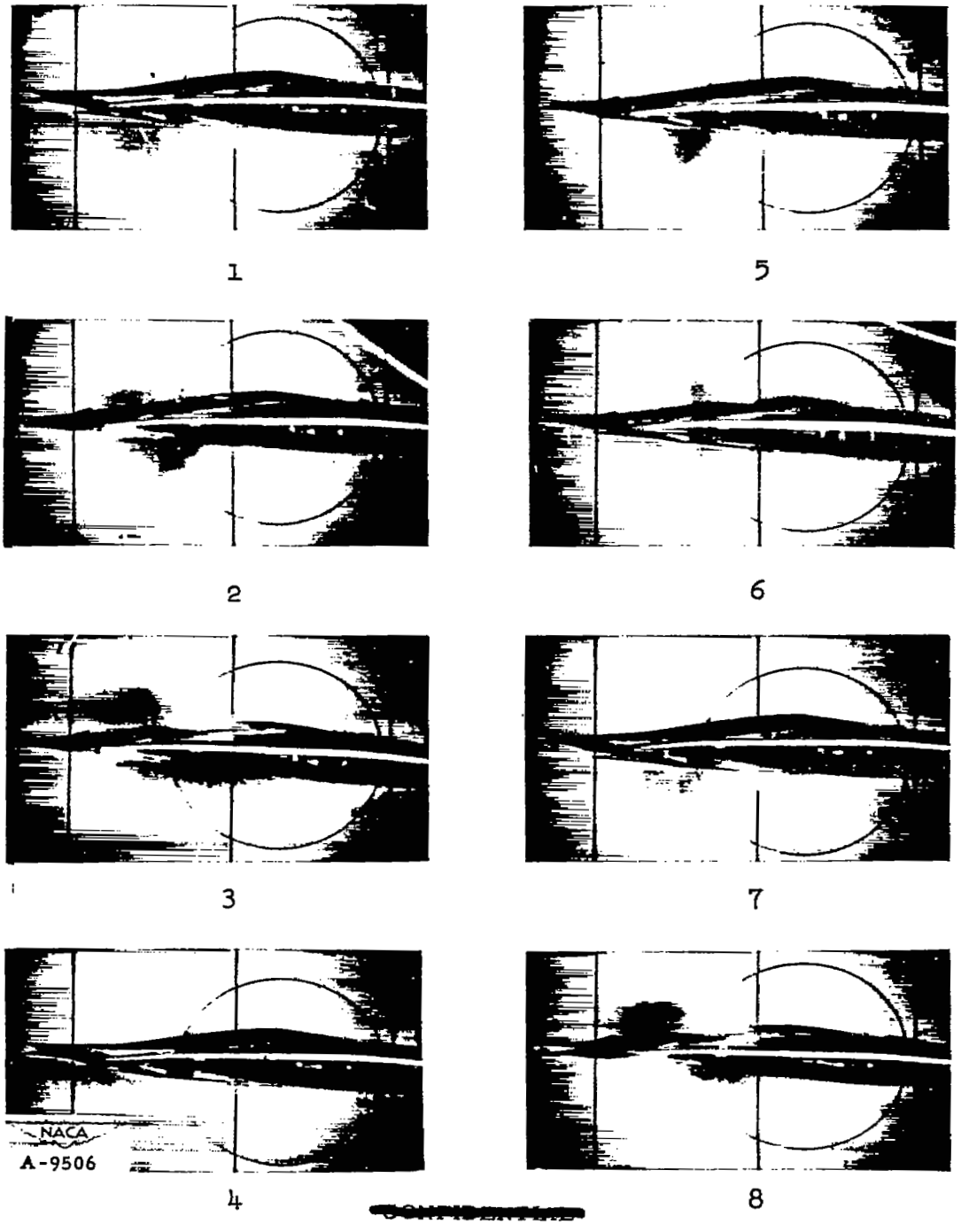

[redacted]

Figure 10.- Shadowgraphs of the wing with the aileron free. Mach number, 0.81; angle of attack, -1°; faired bumps at 50 percent chord on the upper and lower surfaces.

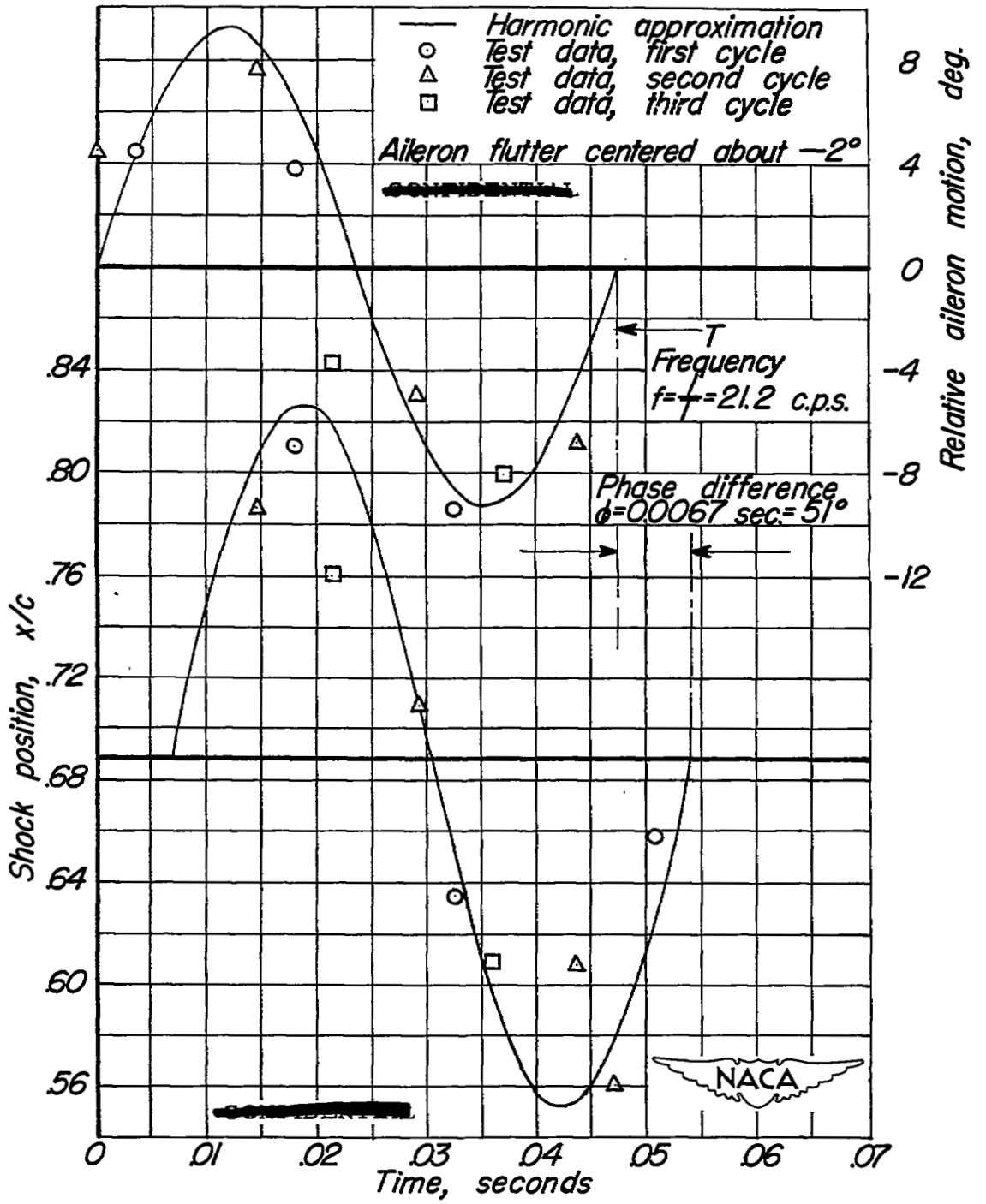

Figure 11.—Variation of aileron angle and normal shock position with time. Mach number, 0.81; angle of attack, −1°; configuration, faired bumps at 50 percent chord on upper and lower surface.

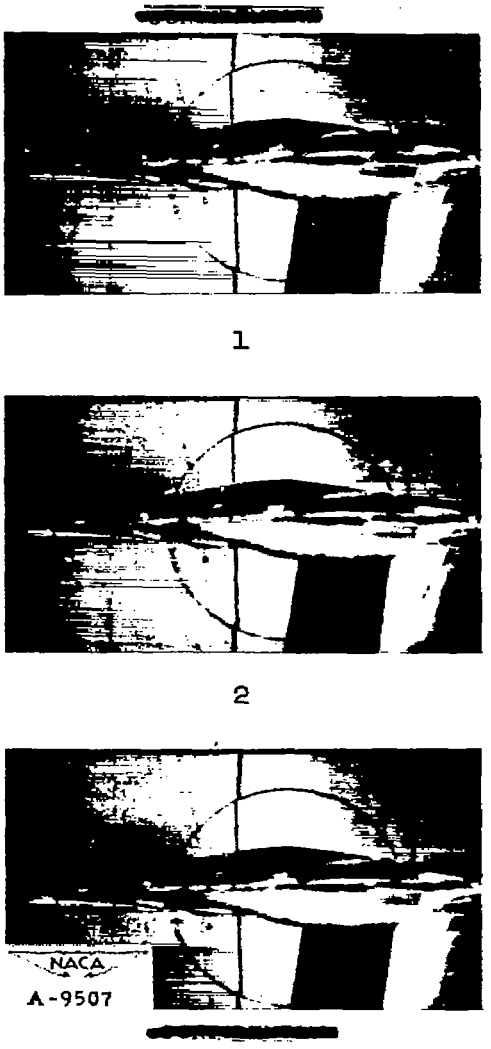

Figure 12.- Consecutive shadowgraphs of the wing with the aileron fixed. Mach number, 0.81; angle of attack, 1°; faired bumps at 70 percent chord on the upper and lower surfaces.

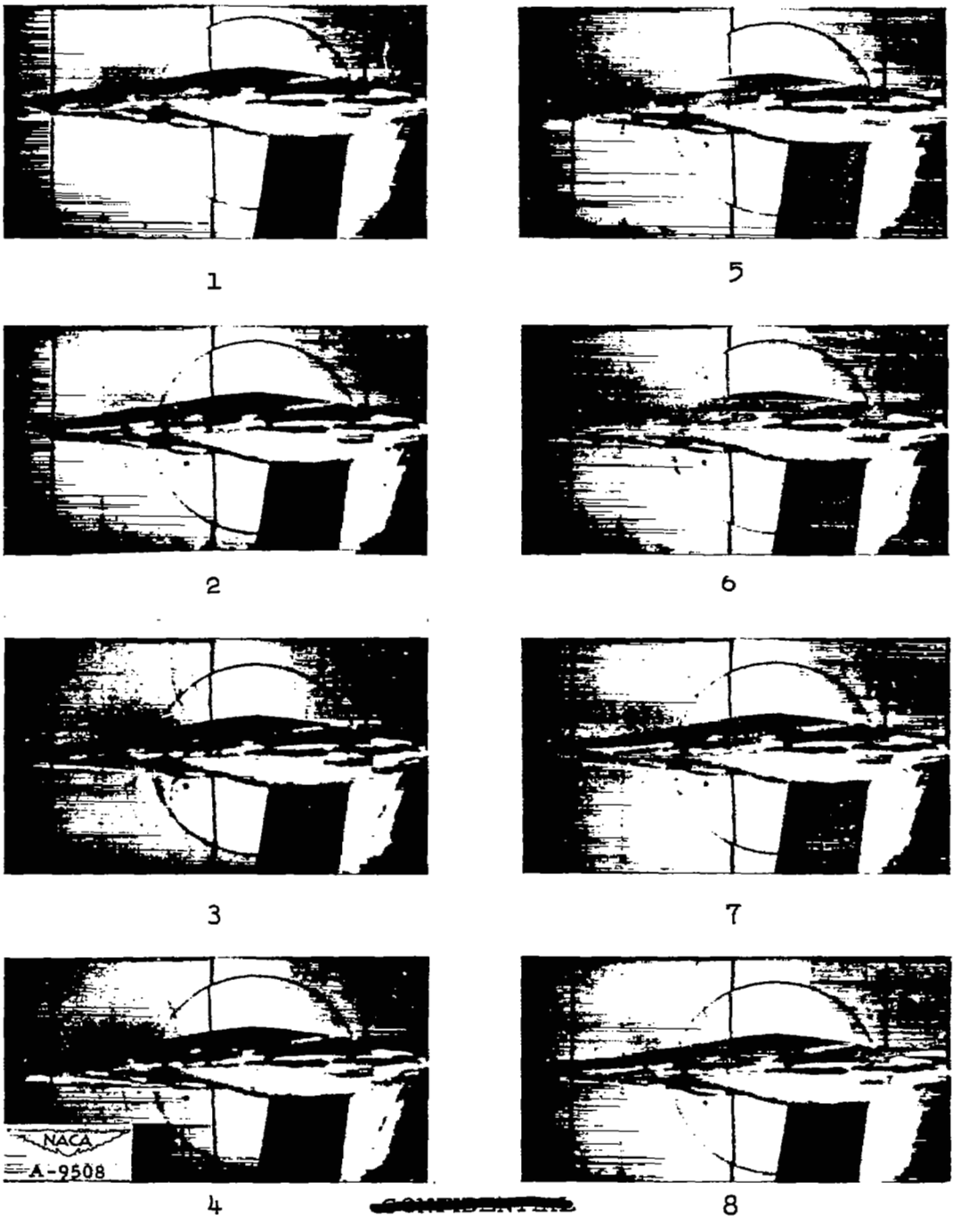

Figure 13.- Shadowgraphs of the wing with the aileron. Mach number, 0.81; angle of attack, 1°; faired bumps at 70 percent chord on the upper and lower surfaces.

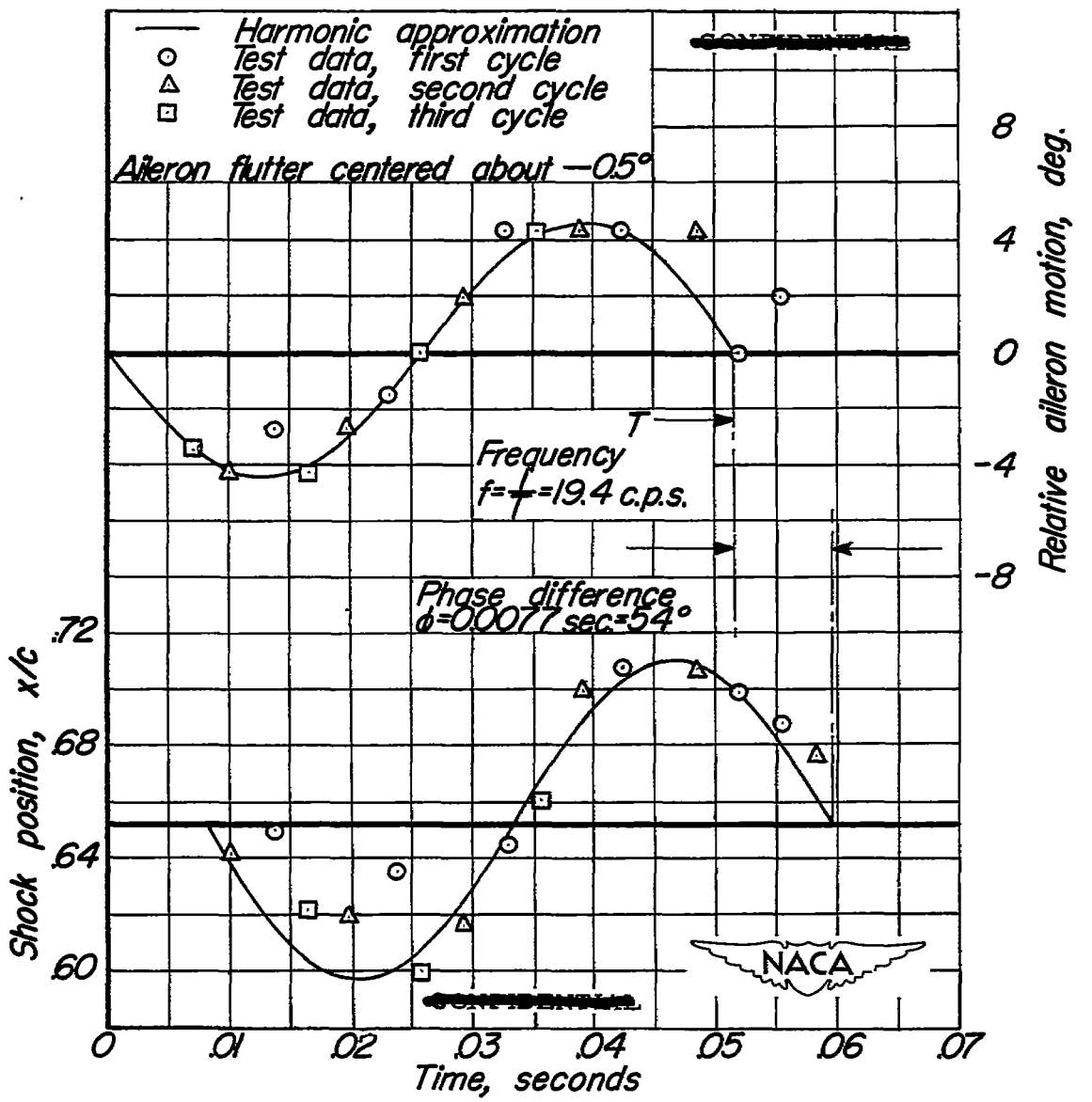

Figure 14.—Variation of aileron angle and normal shock position with time. Mach number, 0.81; angle of attack, 1°; configuration, faired bumps at 70 percent chord on upper and lower surface.

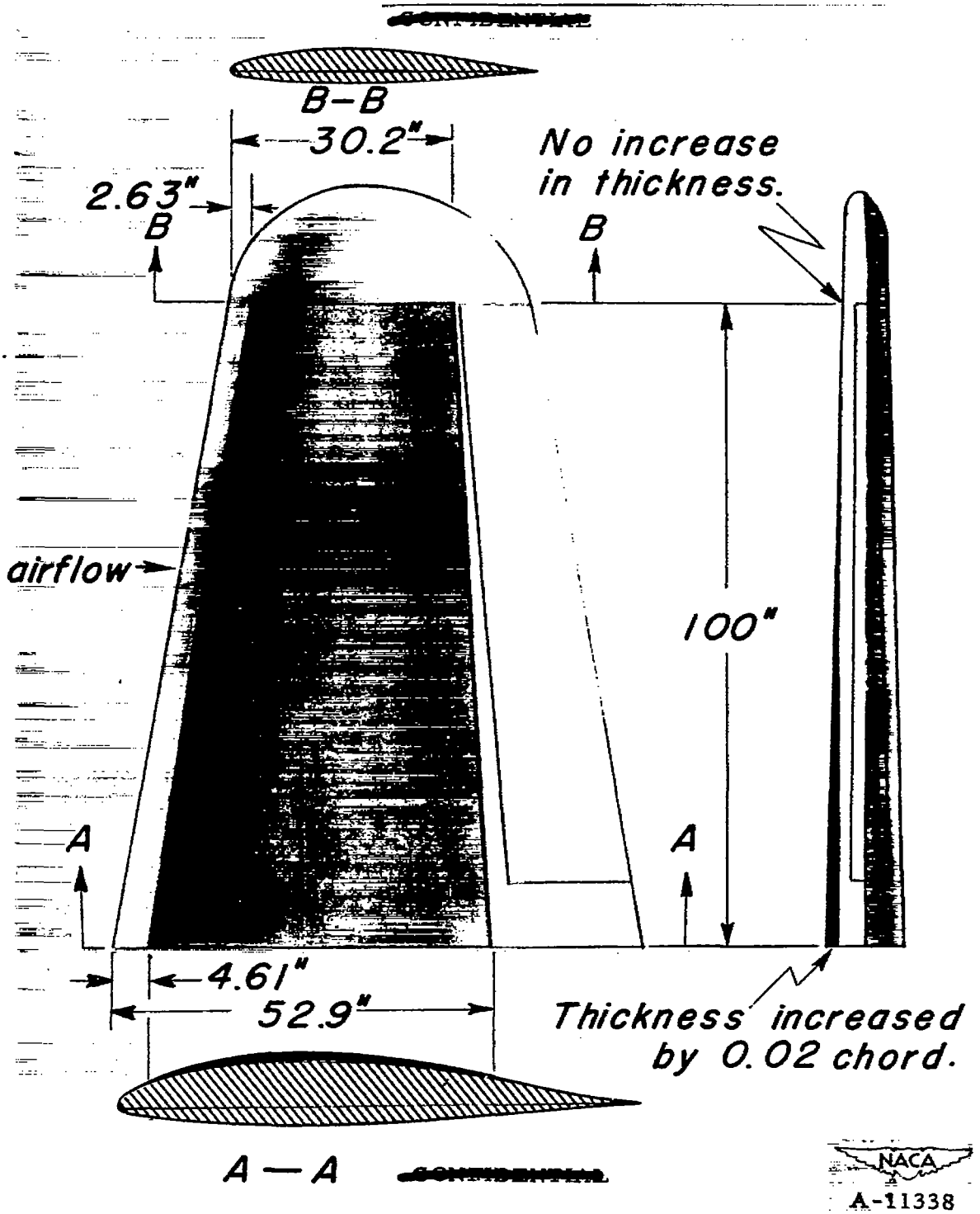

Figure 15.- Thickness taper used to vary the critical Mach number along the span.

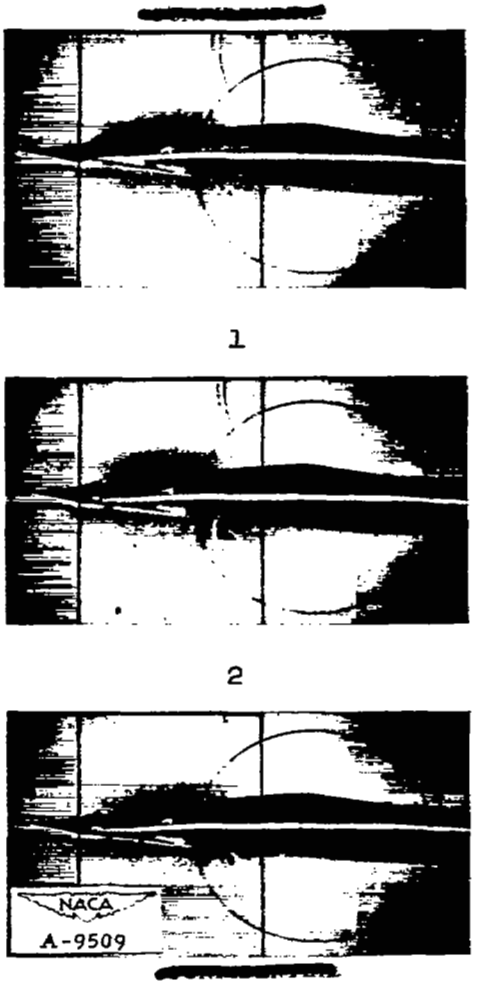

Figure 16.- Consecutive shadowgraphs of the wing with the aileron fixed. Mach number, 0.81; angle of attack, -1°; thickness ratio of wing varying along the span.

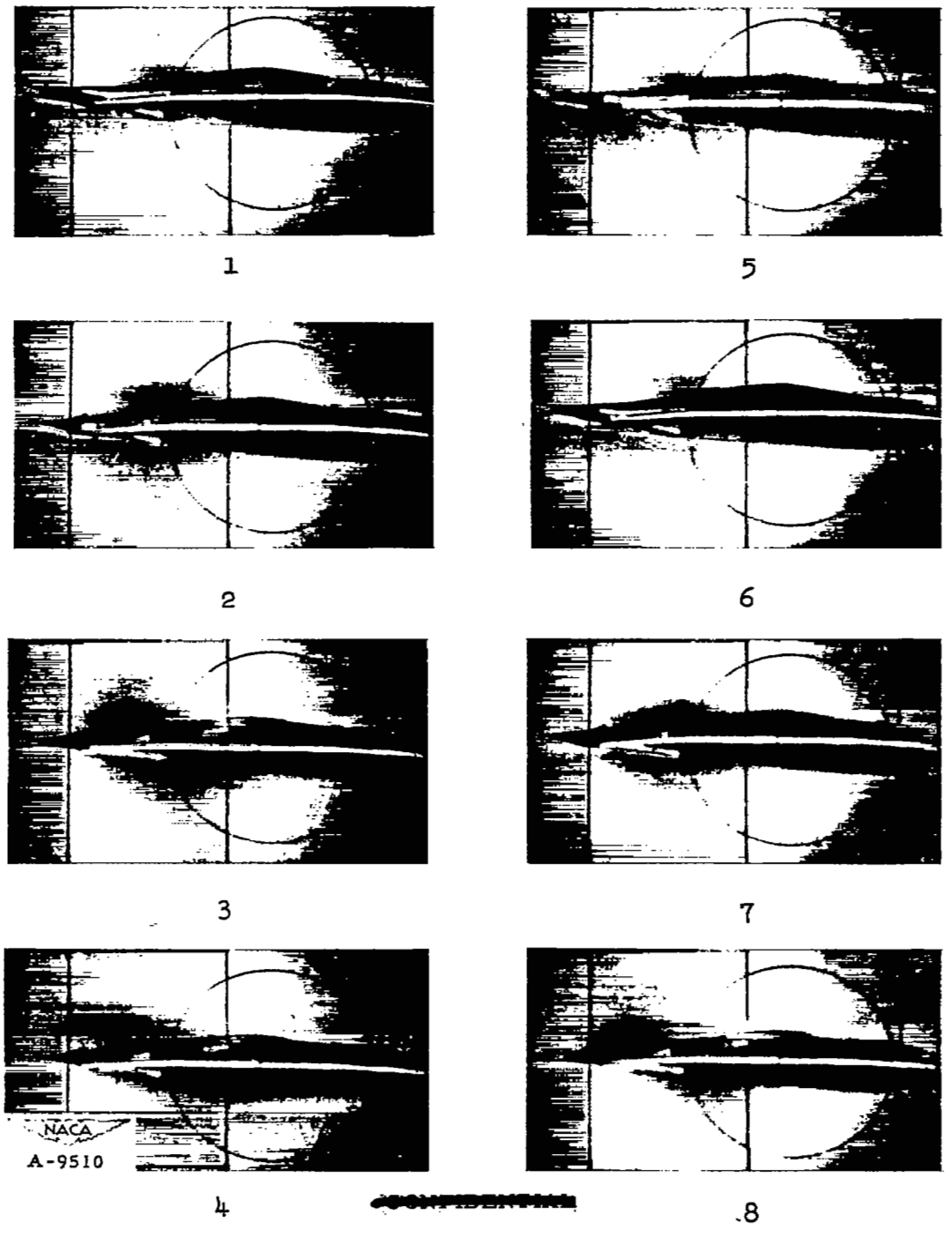

Figure 17.- Shadowgraphs of the wing with the aileron free. Mach number, 0.81; angle of attack, -1°; thickness ratio of wing varying along the span.

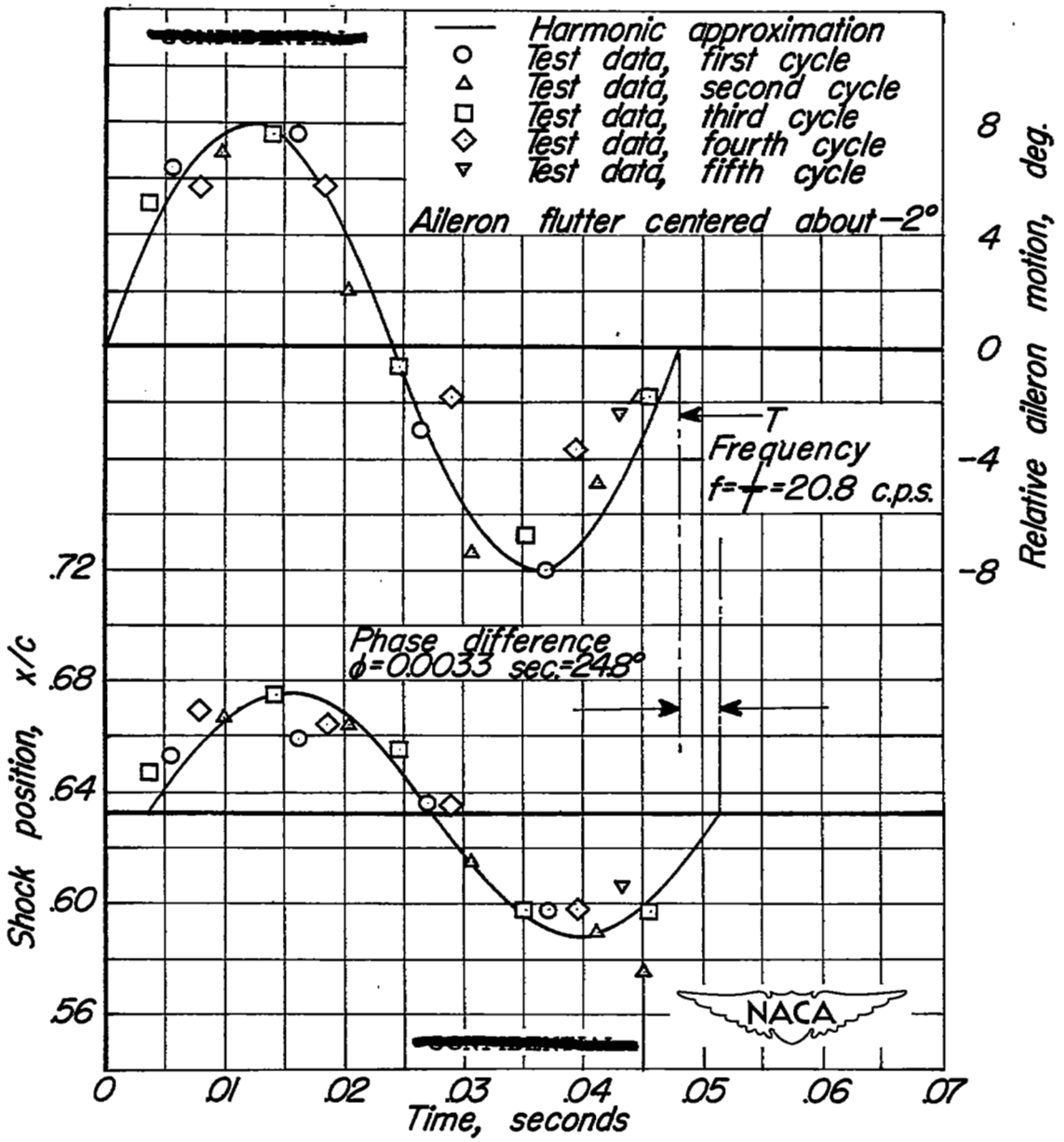

Figure 18.—Variation of aileron angle and normal shock position with time. Mach number, 0.81; angle of attack, −1°; configuration, wing thickness ratio varying along span.

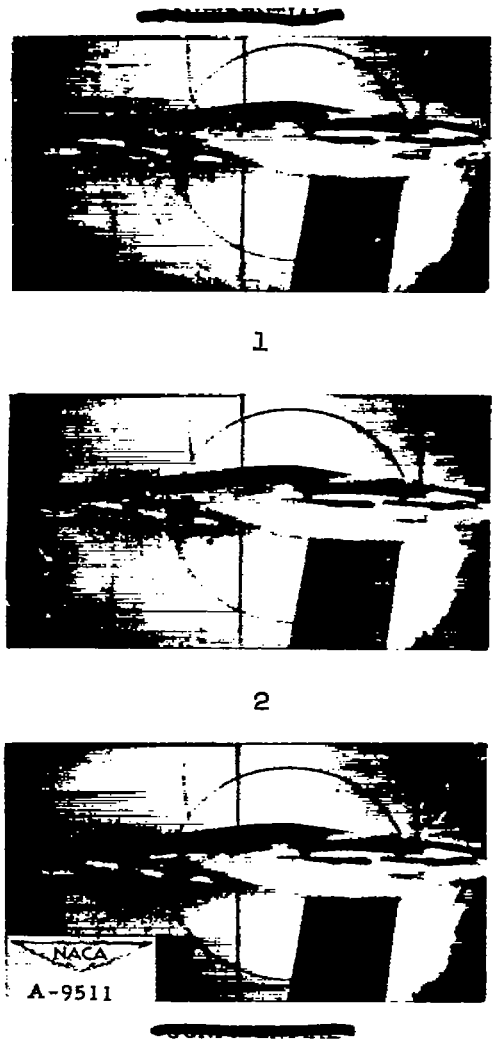

Figure 19.- Consecutive shadowgraphs of the wing with the aileron fixed. Mach number, 0.80; angle of attack, -1°; 39 holes of 15/16-inch diameter in the upper surface near the aileron.

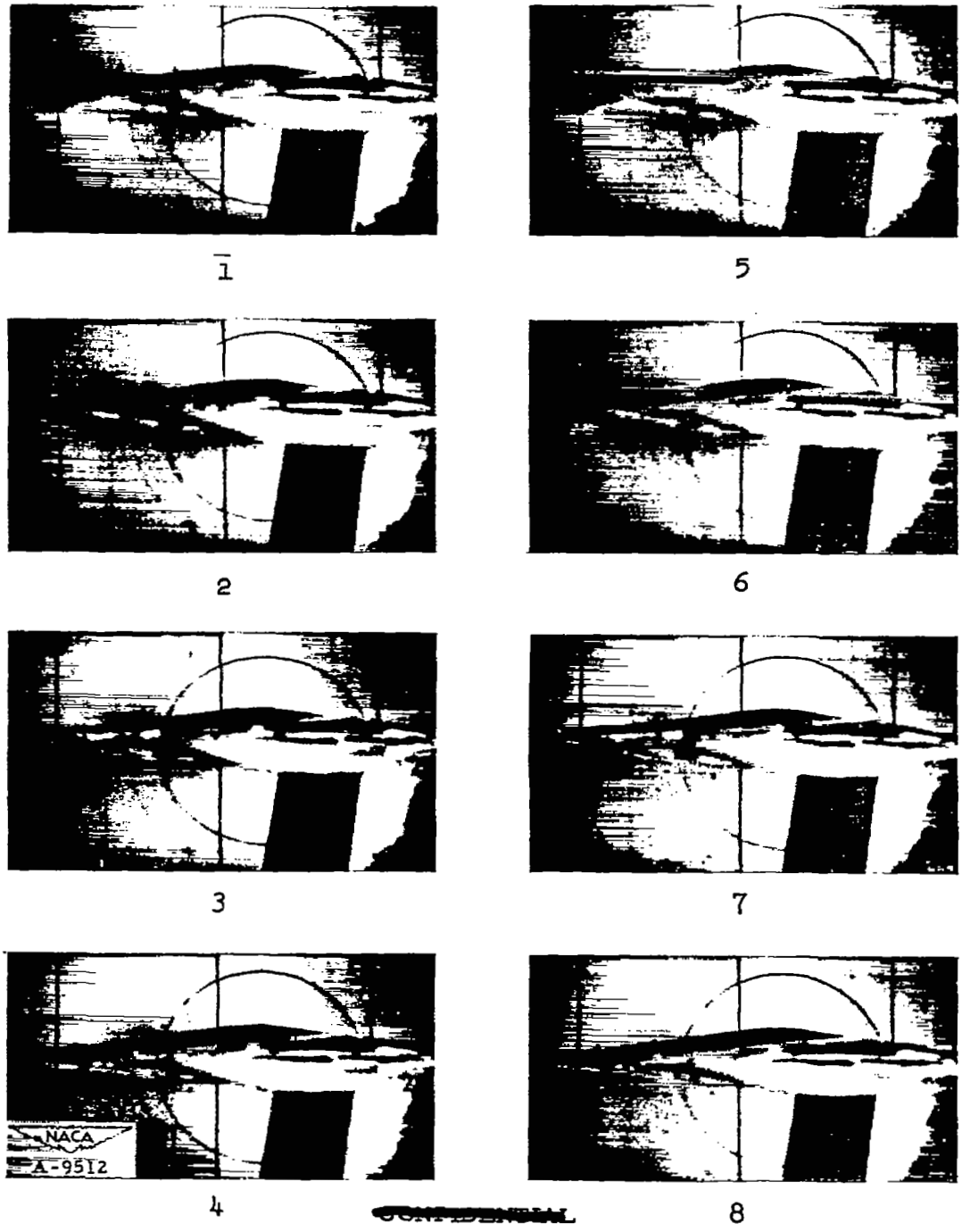

Figure 20.- Shadowgraphs of the wing with the aileron free. Mach number, 0.80; angle of attack, -1°; 39 holes of 15/16-inch diameter in the upper surface near the aileron.

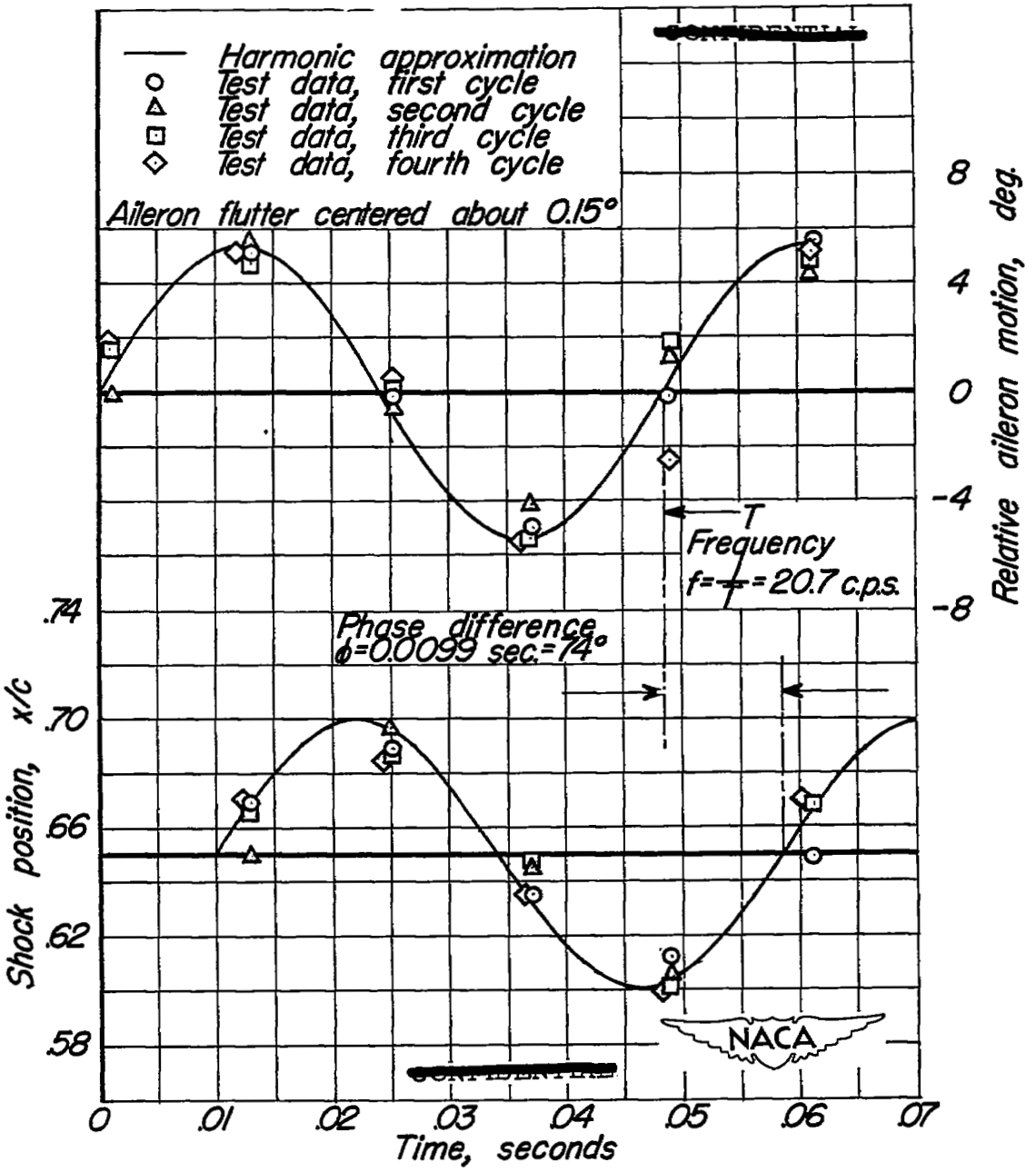

Figure 21.—Variation of aileron angle and normal shock position with time. Mach number, 0.80; angle of attack, —1°; configuration, 39 holes of 15/16 inch diameter in upper surface 3 inches forward of the hinge line.

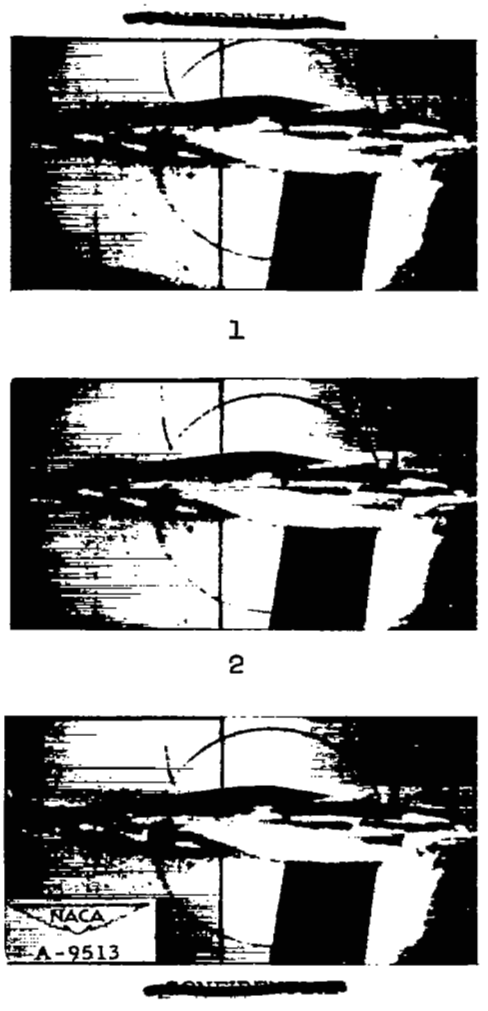

Figure 22.- Consecutive shadowgraphs of the wing with the aileron fixed. Mach number, 0.80; angle of attack, -1°; 39 holes in upper surface and 15 holes in lower surface near the aileron; diameter, 15/16 inches.

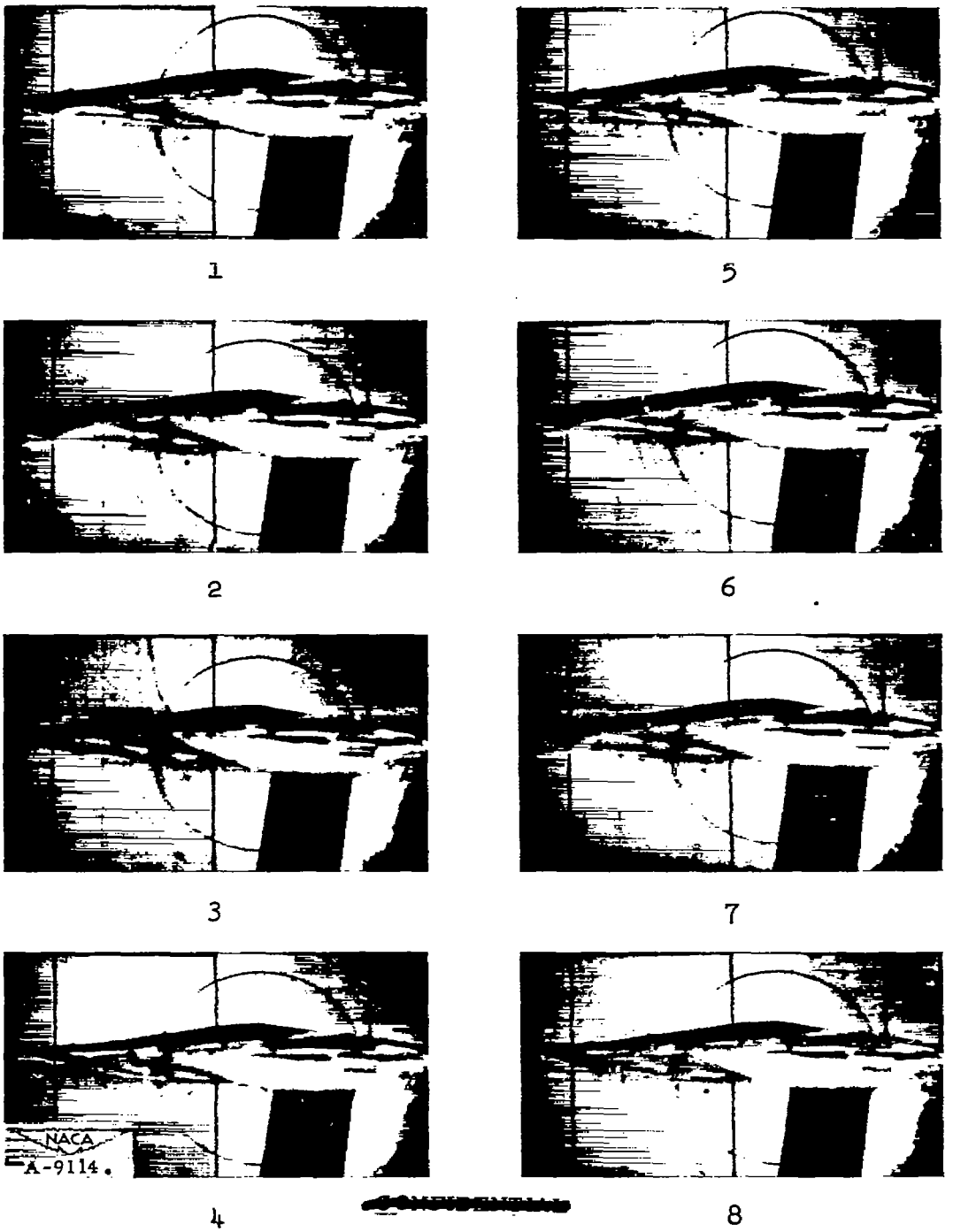

Figure 23.- Shadowgraphs of the wing with the aileron free. Mach number, 0.80; angle of attack, -1°; 39 holes in upper surface and 15 holes in lower surface near the aileron; diameter, 15/16 inches.

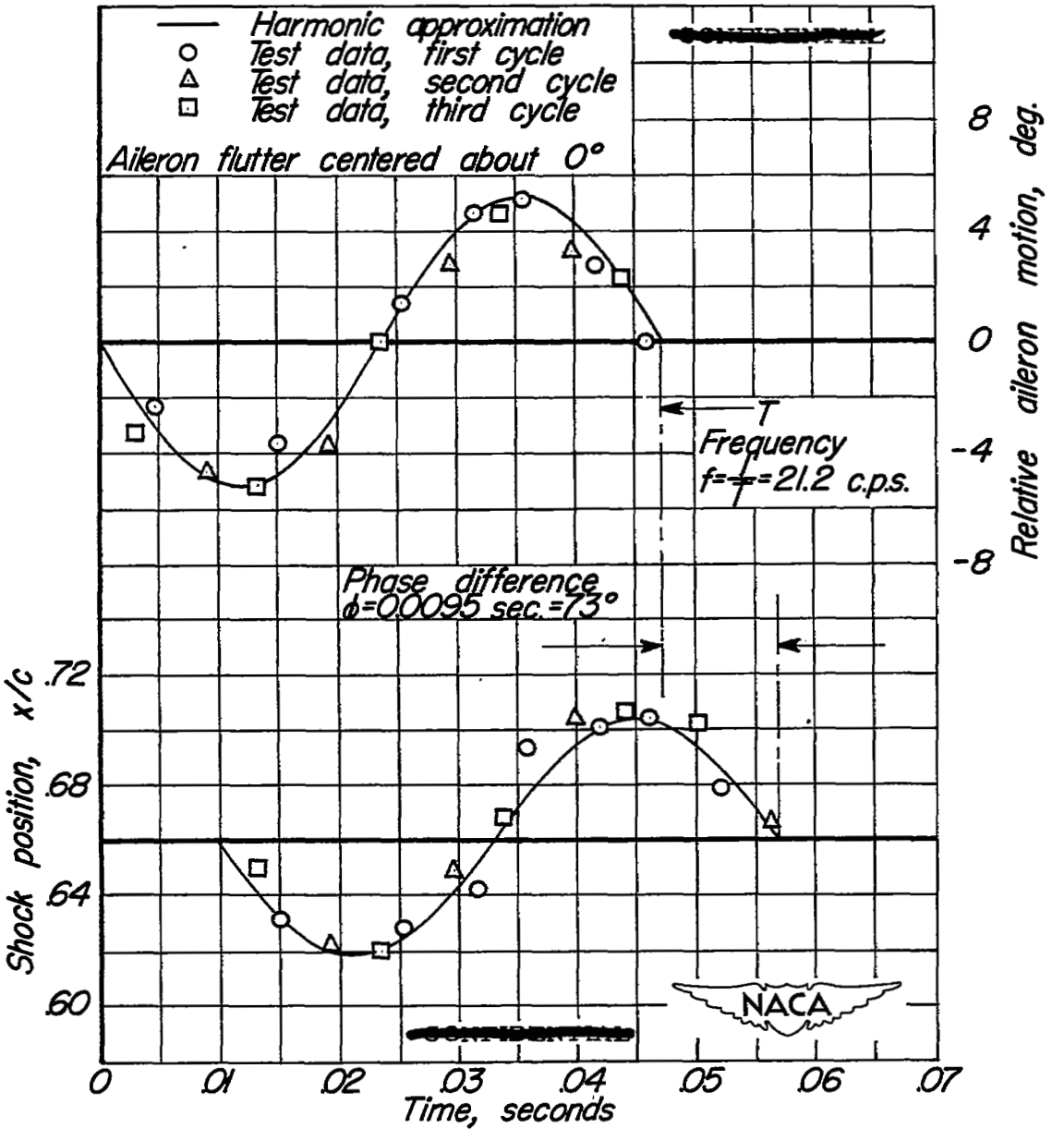

Figure 24.—Variation of aileron angle and normal shock position with time. Mach number, 0.80; angle of attack, —1°; configuration, 39 holes 15/16 inches in diameter in the upper surface and 15 holes 15/16 inches in diameter in the lower surface near the aileron.

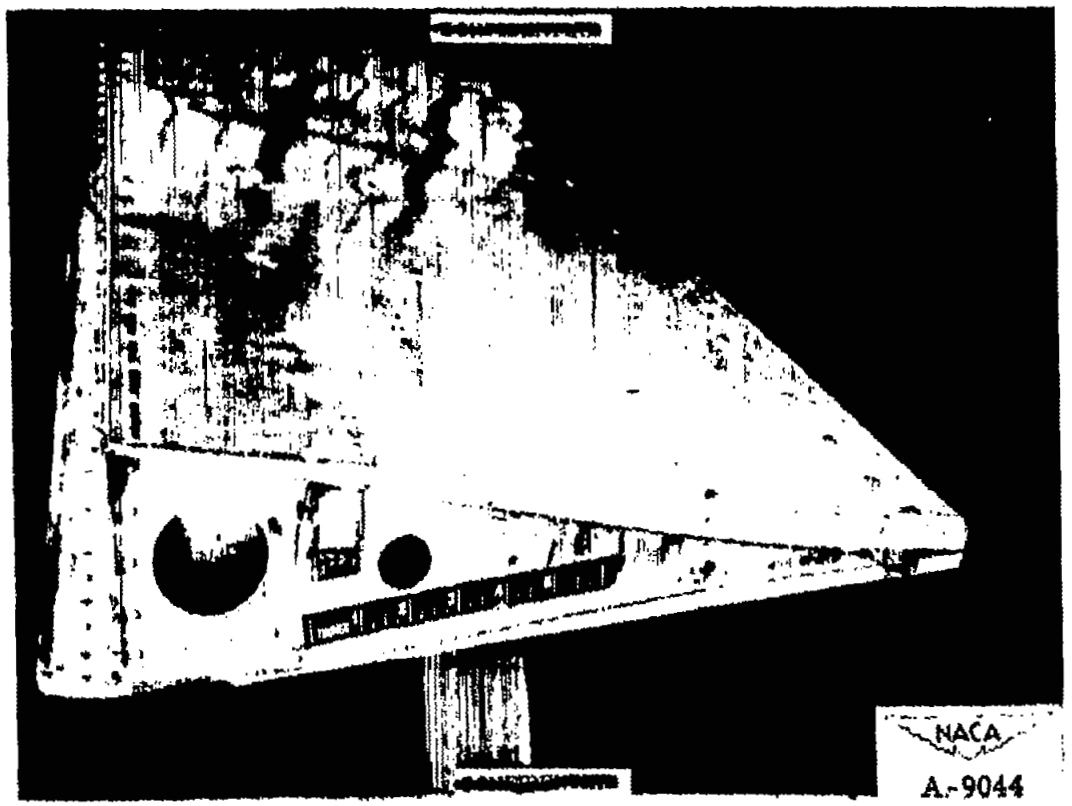

Figure 25.- Inboard end of aileron with built-up flat-sided section and blunt trailing edge.

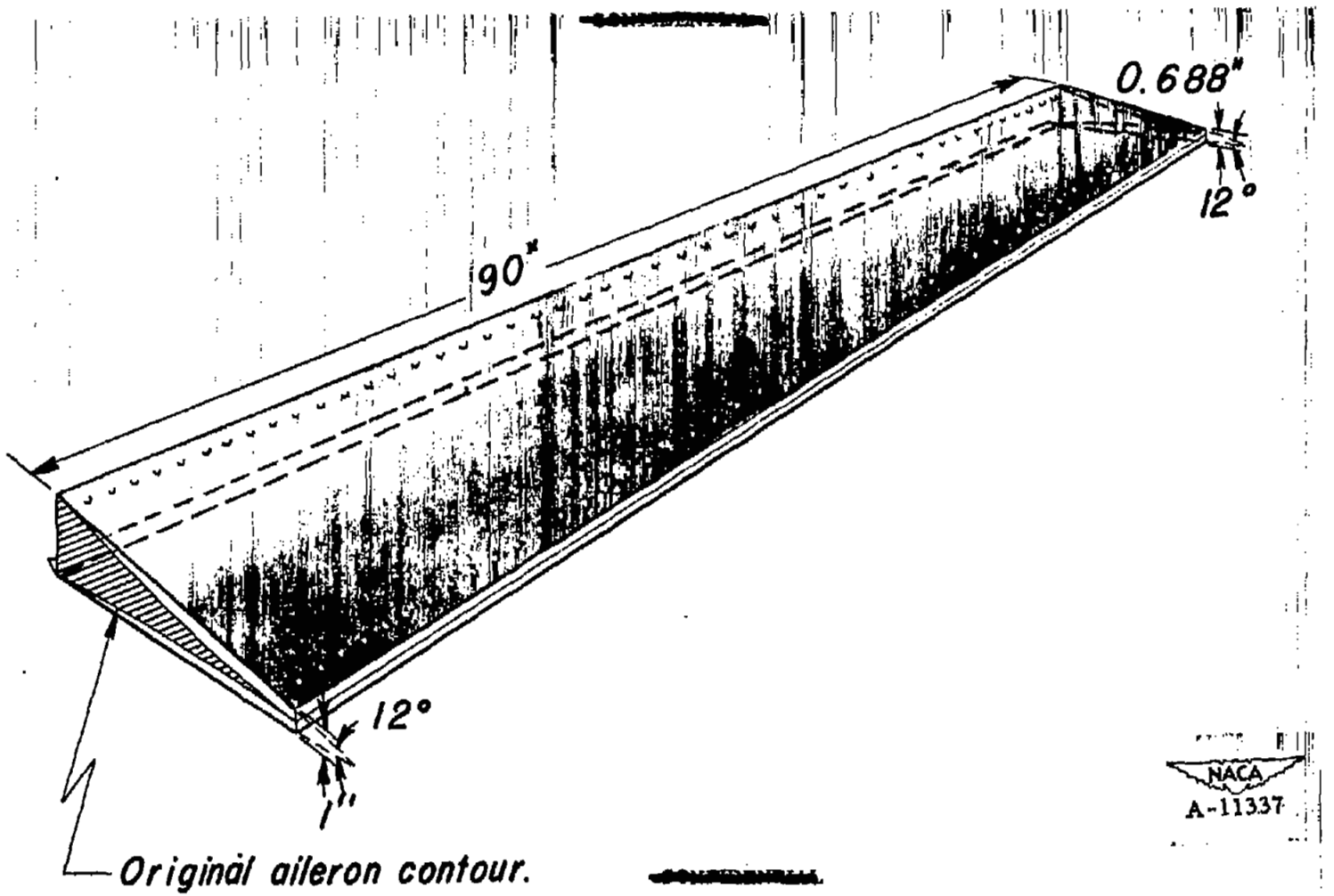

Figure 26.- Dimensions of built-up flat-sided section with blunt trailing edge.

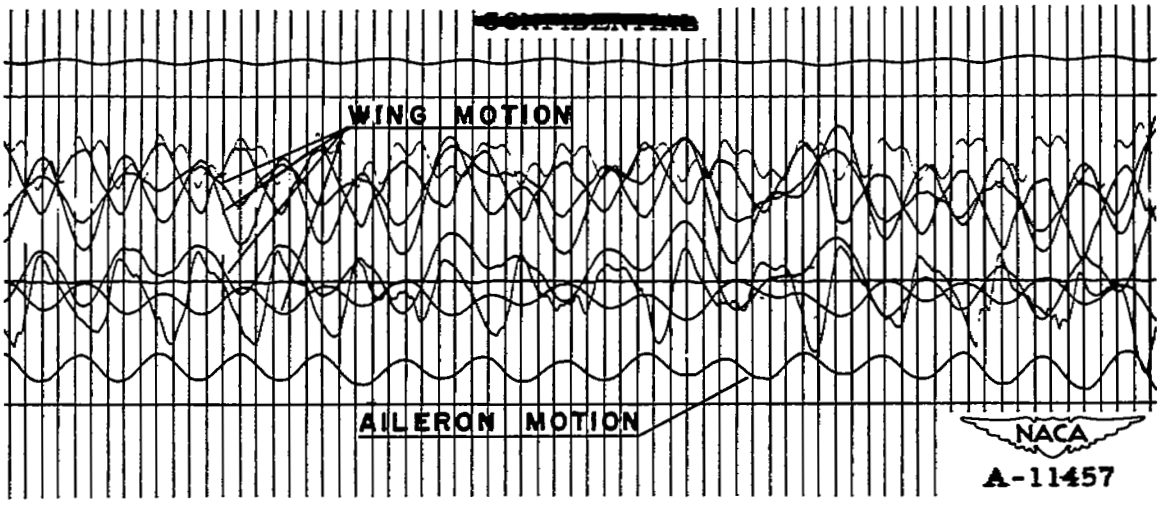

(a) Flutter at 20.6 cycles per second.

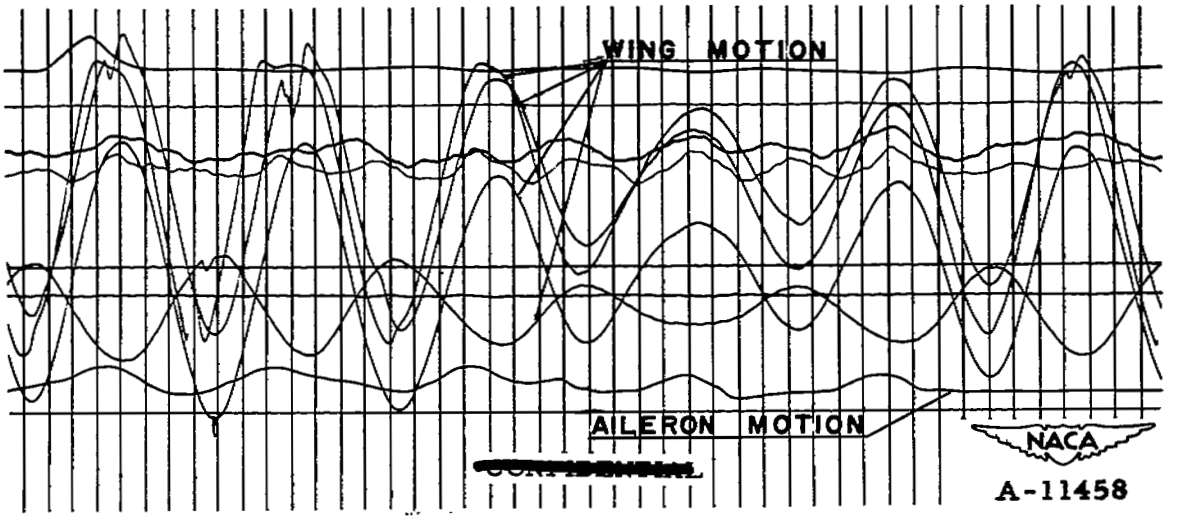

(b) Flutter at 13 cycles per second.

Figure 27.- Oscillograms for the standard wing and aileron showing change from basic aileron motion to wing motion. Mach number, 0.825; angle of attack, -1°.

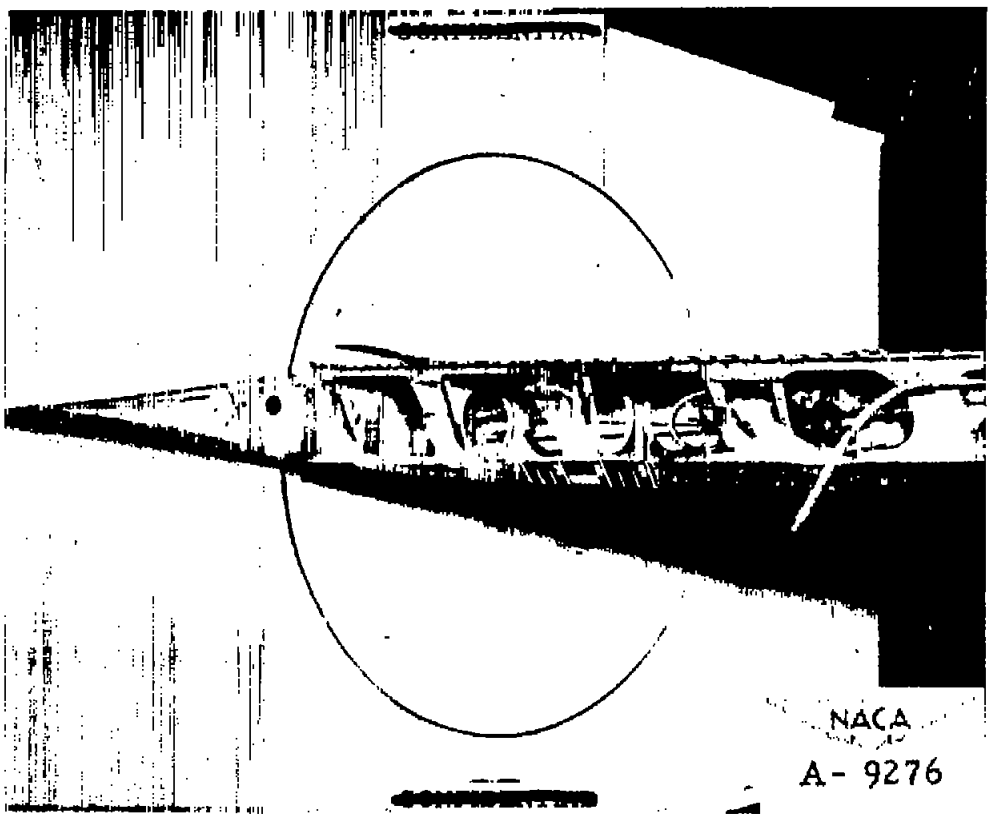

Figure 28.- Damage to the wing which resulted from or was the cause of the flutter at 13 cycles per second. The picture shows the wing with aileron removed.

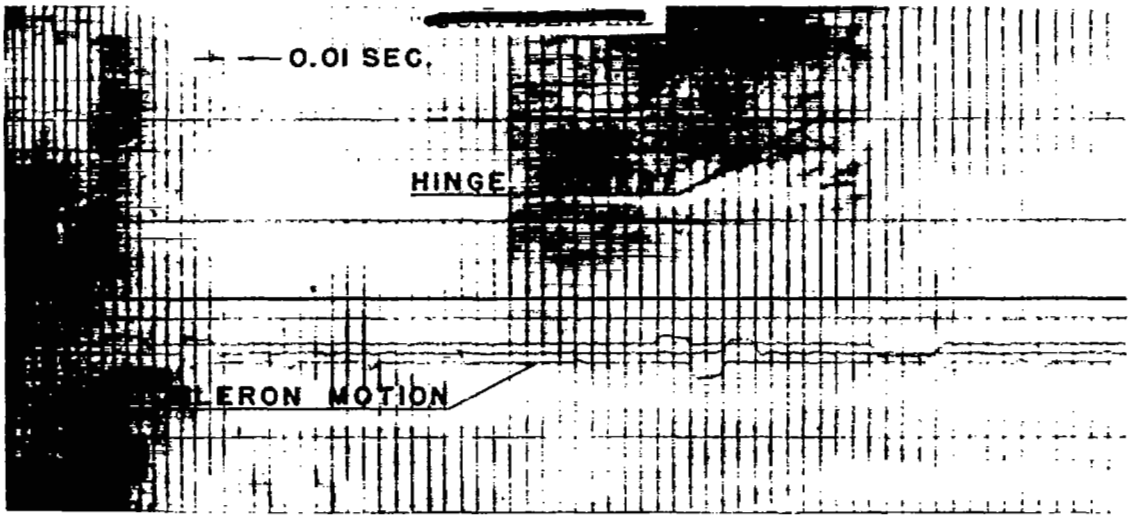

(a) Mach number 0.75.

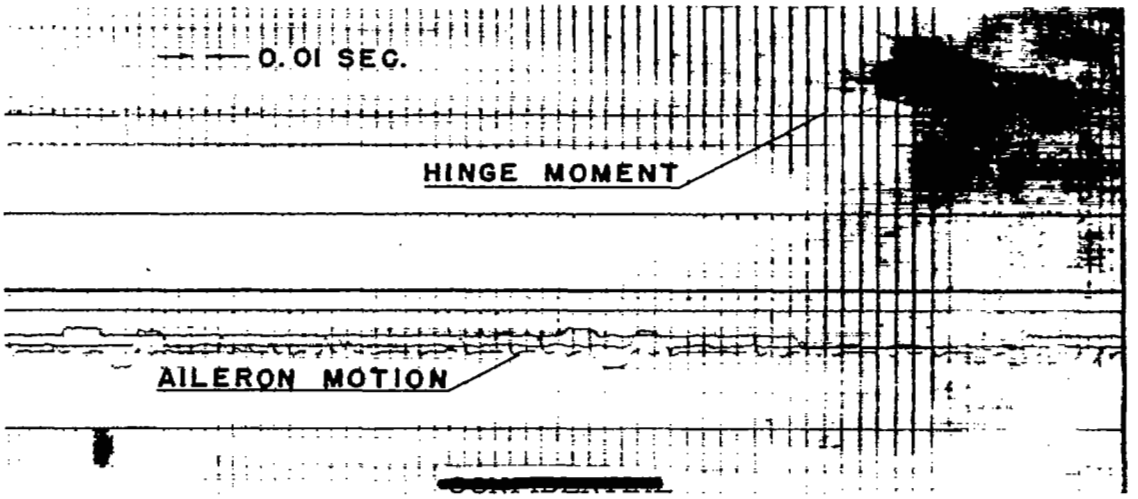

(b) Mach number 0.775.

Figure 29.- Records of buffeting hinge moments. Angle of attack, -1°; aileron angle approximately, -2°.

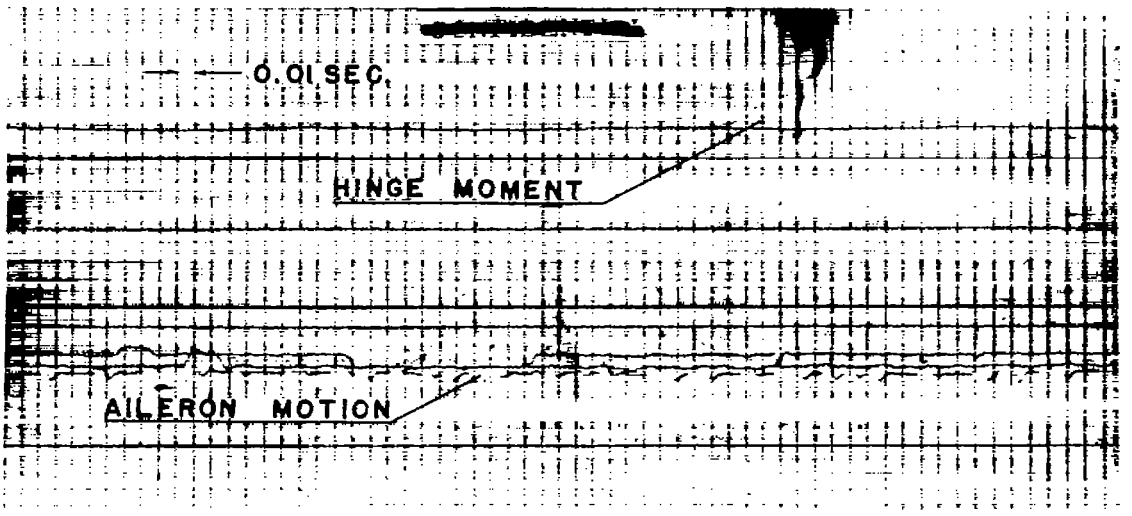

(c) Mach number 0.80.

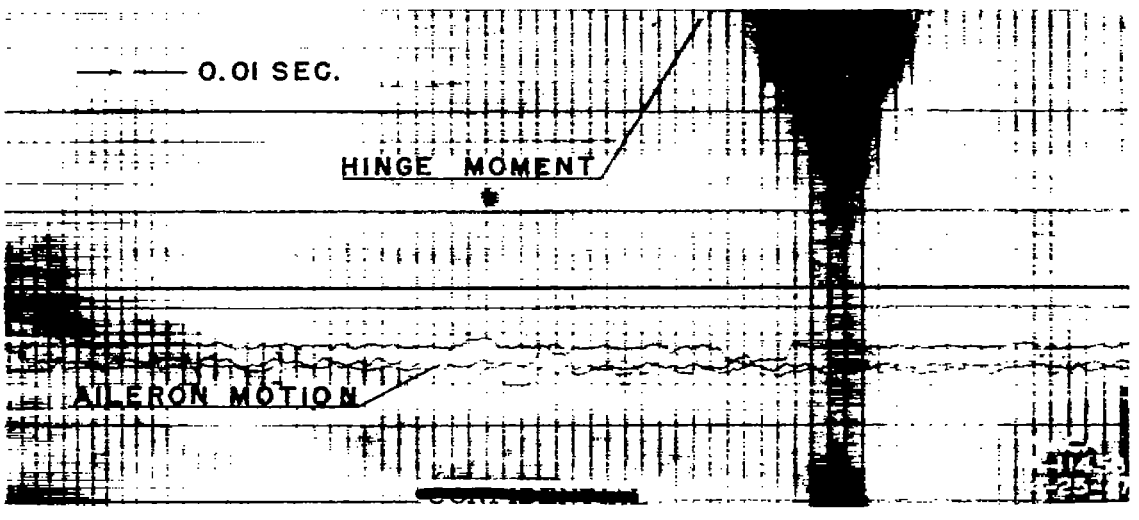

(d) Mach number 0.825.

Figure 29.- Concluded.

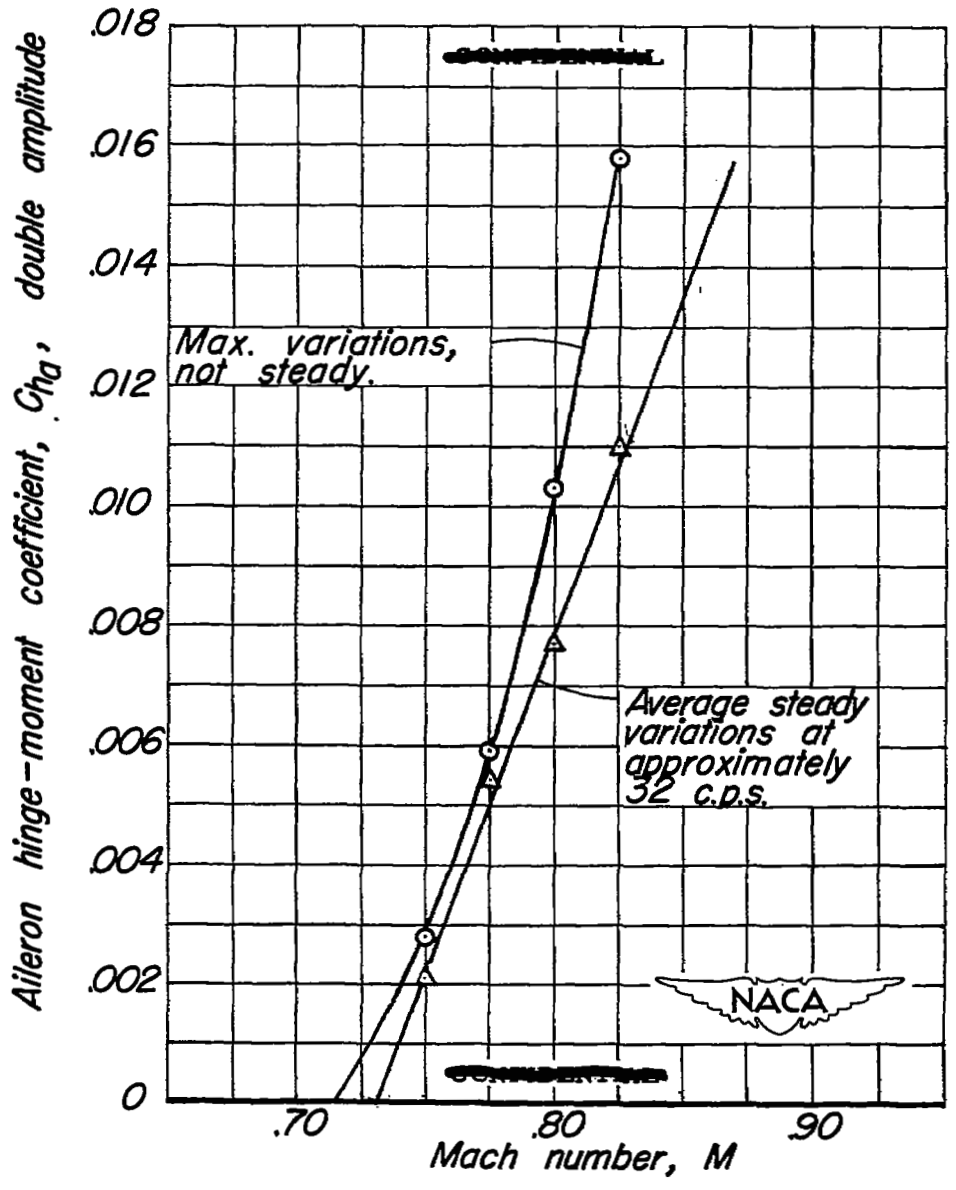

Figure 30.—Buffeting hinge moments with aileron restrained.

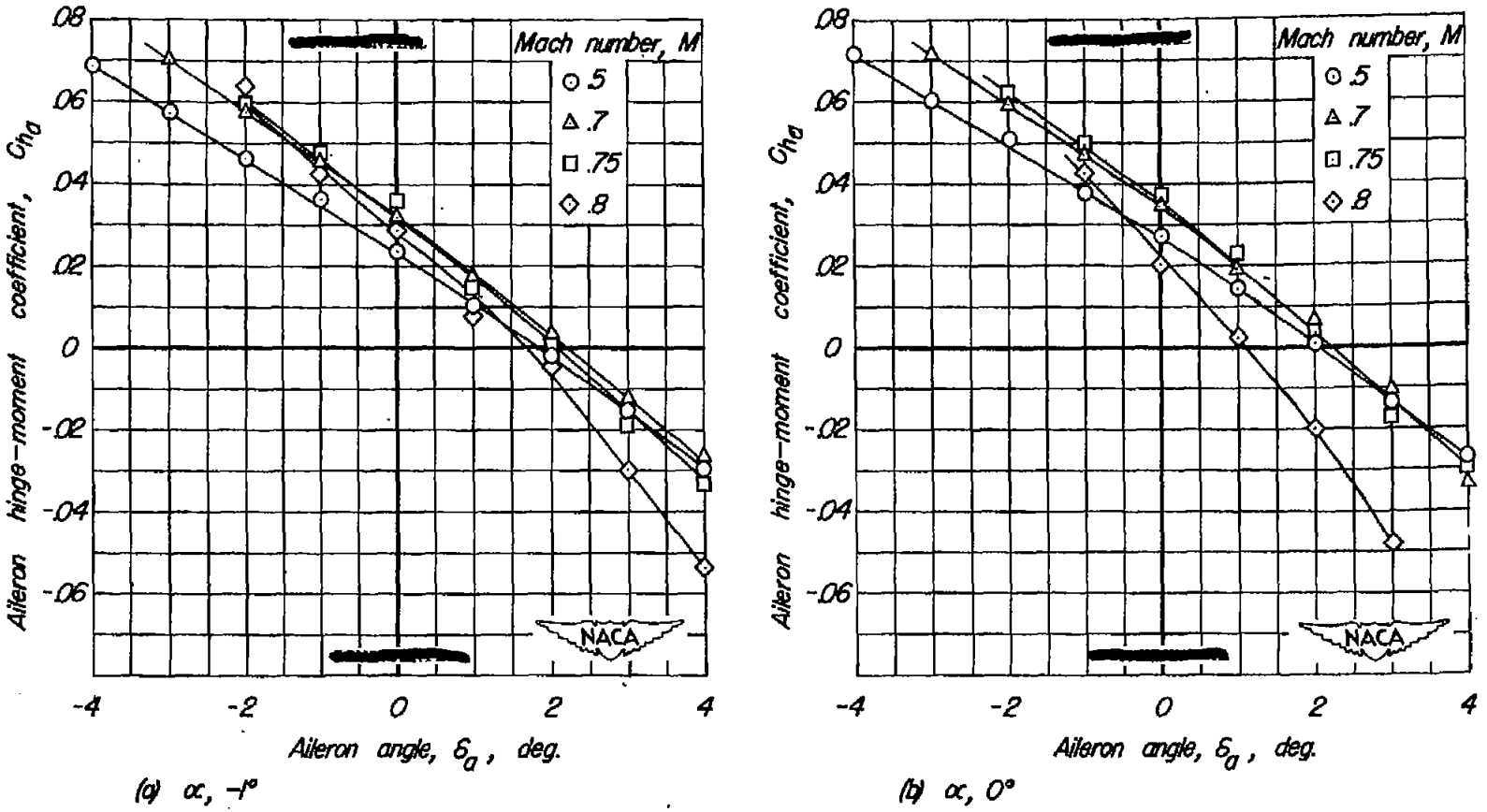

Figure 31.—Variation of aileron hinge-moment coefficient with aileron angle at several Mach numbers.

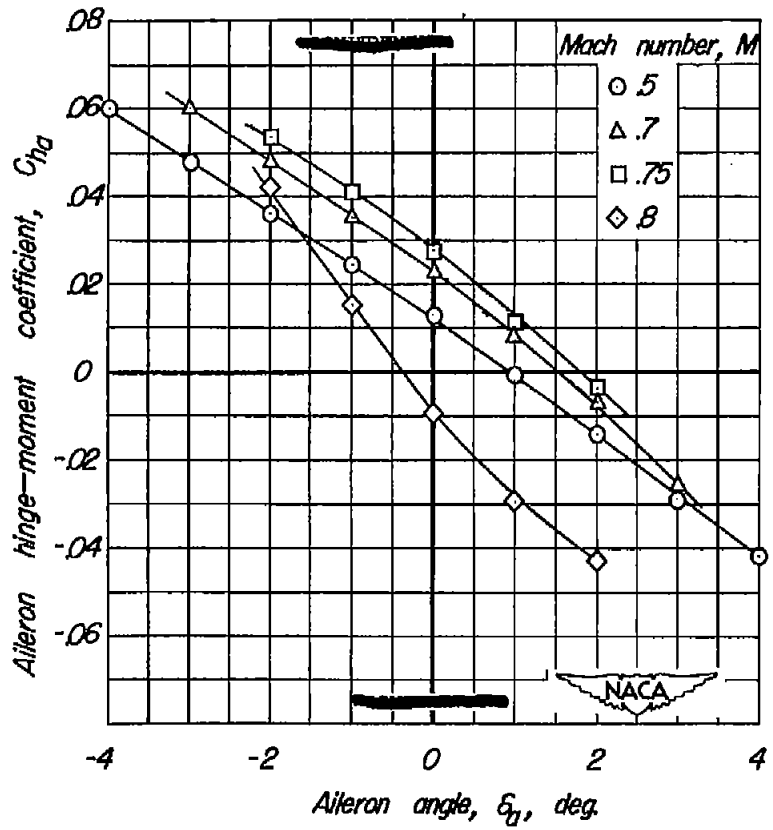

(c) α, 1°

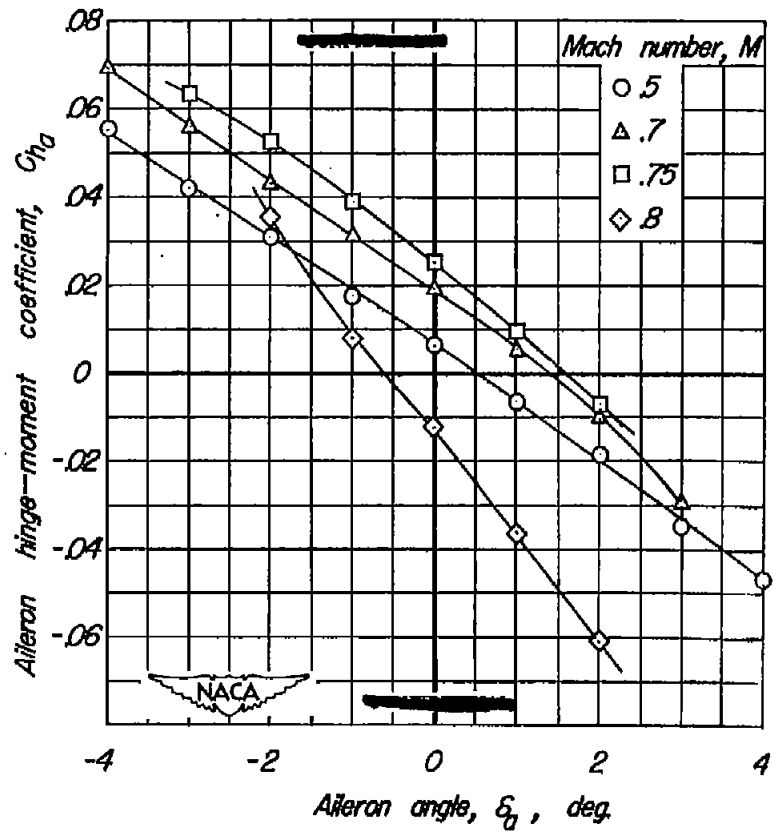

(d) α, 2°

Figure 31.—Concluded.

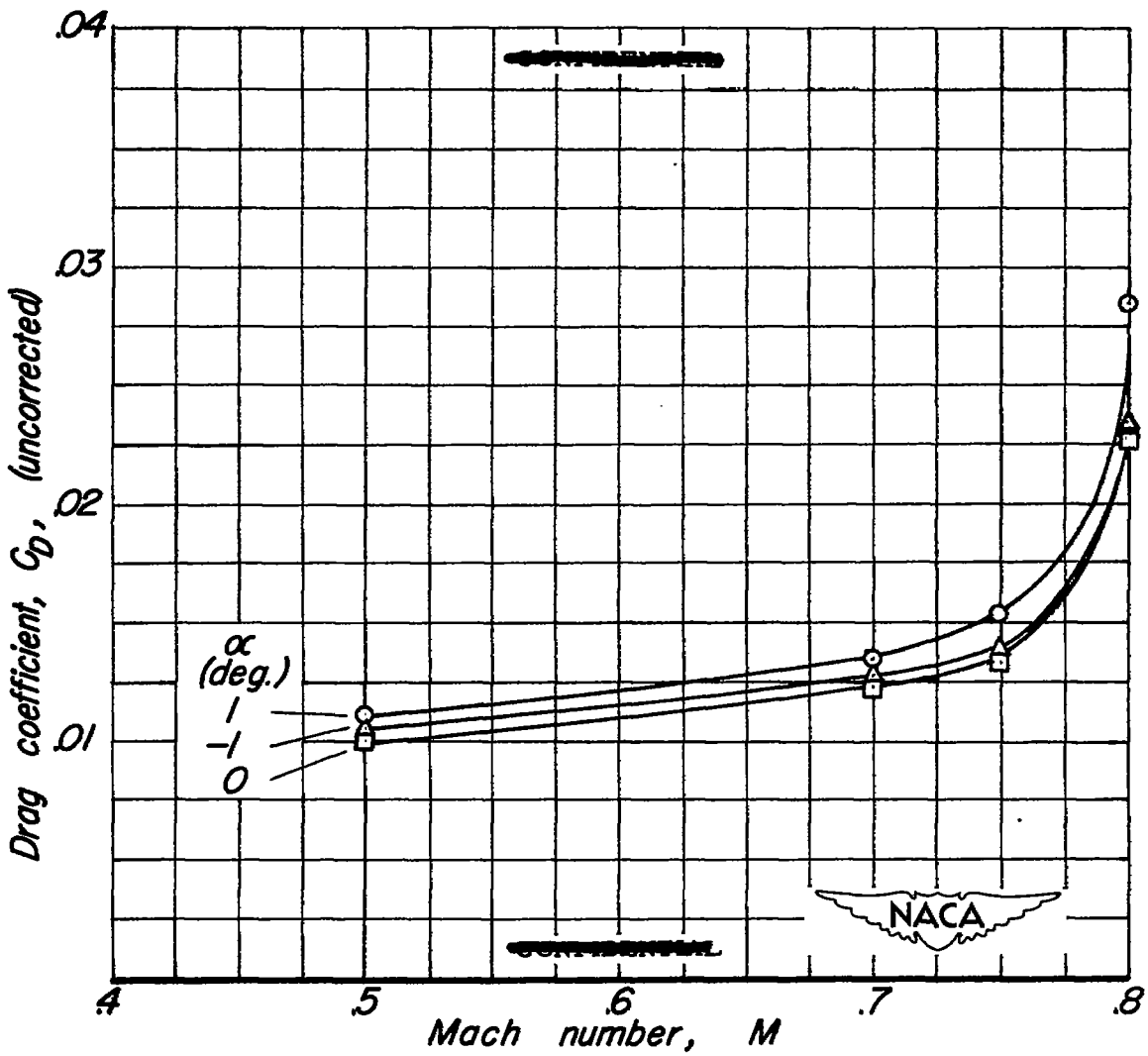

Figure 32—Variation of the drag coefficient with Mach number for the standard configuration.

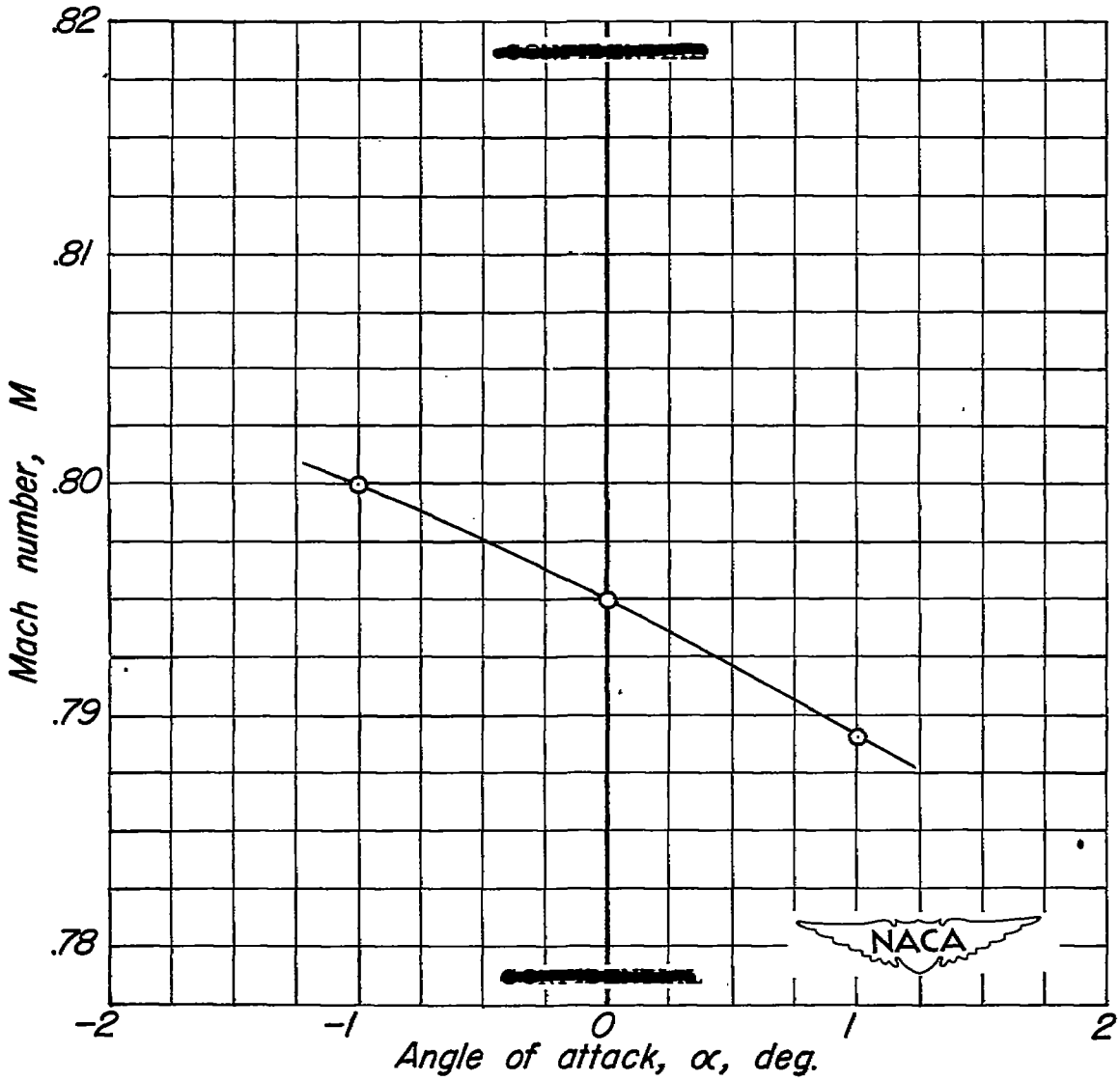

Figure 33.—Variation of Mach number at which flutter occurred with angle of attack for the standard configuration with aileron free.

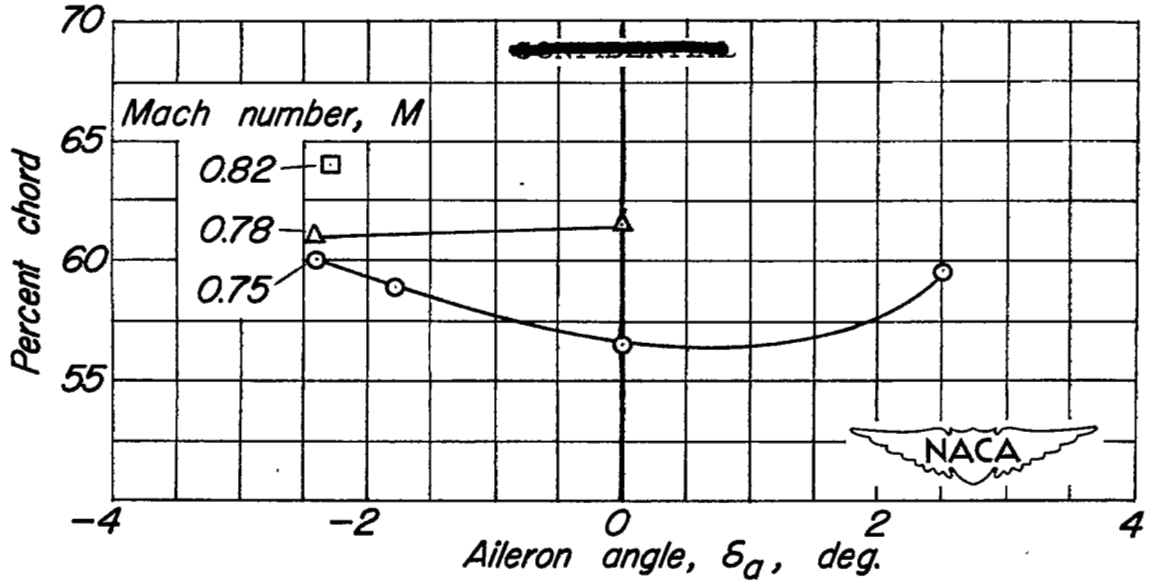

(a) α, 1°.

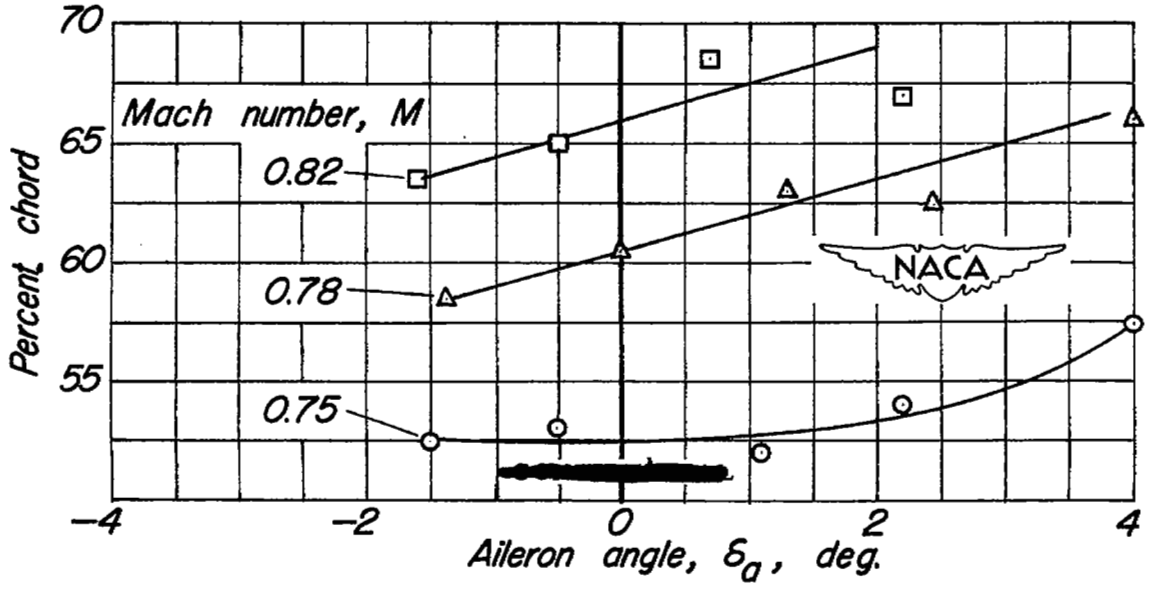

(b) α, −1°

Figure 34.—Location of upper surface shock wave under static conditions.